nature chemical biology

ARTICLES

https://doi.org/10.1038/s41589-021-00913-4



# Dynamic eIF3a *O*-GlcNAcylation controls translation reinitiation during nutrient stress

Xin Erica Shu, Yuanhui Mao, Longfei Jia and Shu-Bing Qian ✉

**In eukaryotic cells, many messenger RNAs (mRNAs) possess upstream open reading frames (uORFs) in addition to the main coding region. After uORF translation, the ribosome could either recycle at the stop codon or resume scanning for downstream start codons in a process known as reinitiation. Accumulating evidence suggests that some initiation factors, including eukaryotic initiation factor 3 (eIF3), linger on the early elongating ribosome, forming an eIF3–80S complex. Very little is known about how eIF3 is carried along with the 80S during elongation and whether the eIF3–80S association is subject to regulation. Here, we report that eIF3a undergoes dynamic *O*-linked *N*-acetylglucosamine (*O*-GlcNAc) modification in response to nutrient starvation. Stress-induced de-*O*-GlcNAcylation promotes eIF3 retention on the elongating ribosome and facilitates activating transcription factor 4 (ATF4) reinitiation. Eliminating the modification site from eIF3a via CRISPR genome editing induces ATF4 reinitiation even under the nutrient-rich condition. Our findings illustrate a mechanism in balancing ribosome recycling and reinitiation, thereby linking the nutrient stress response and translational reprogramming.**

Eukaryotic messenger RNA (mRNA) translation is a highly orchestrated event encompassing initiation, elongation, termination and recycling[1–3]. The small 40S ribosomal subunit binds to the initiator methionyl-tRNA in a ternary complex (TC), forming the 43S preinitiation complex. Following recognition of the 5′-end m$^7$G cap, the preinitiation complex searches for an AUG start codon in the optimal context. Recognition of the start codon triggers a series of events, including dissociation of initiation factors (eIFs) and joining of the large 60S ribosomal subunit. Assembly of the 80S ribosome at the start codon is followed by elongation, a cyclic decoding process that is repeated until the elongating ribosome encounters a stop codon. Assisted by release factors and other recycling factors, translation termination involves peptide discharge, ribosome splitting and mRNA release. In some cases, however, termination at the stop codon is followed by reinitiation in which the ribosome remains bound to the mRNA and resumes scanning for downstream start codons[4]. Reinitiation is often used by viruses to express several open reading frames (ORFs) from one mRNA. Some cellular mRNAs harboring upstream open reading frames (uORFs) are also capable of reinitiation, especially under stress conditions. The best characterized example is *GCN4* in yeast and *ATF4* in mammals[5–7], whose translation is selectively induced during amino acid deprivation. The stress-responsive feature underscores the physiological importance of translation reinitiation in enabling cells to adapt to changing environmental conditions.

For transcripts with multiple ORFs, the reinitiation potency is highly dependent on *cis*-sequence elements and *trans*-acting factors. It has been reported that reinitiation efficiency is inversely correlated with the length of the uORF[8]. In addition, stable secondary structures in the uORF negatively influence the reinitiation potential[9]. These observations suggest that increased duration of uORF translation might ultimately lead to the loss of reinitiation capability of the ribosome upon termination. Beside uORF length, the distance between the uORF stop codon and the downstream coding region (CDS) start codon is also crucial[8]. It has been suggested that a minimal rescanning time is needed for the post-termination ribosome to acquire an initiator methionyl-tRNA from the TC[10]. Because TC availability largely determines how far the 40S subunit could migrate, delayed TC acquisition has evolved as a central mechanism for stress-induced translation reinitiation[5]. The integrated stress response, by sensing several distinct stress conditions, converges on eIF2α phosphorylation that reduces TC availability[11]. As a result, global translation is attenuated, and the synthesis of stress proteins is upregulated via translation reinitiation. However, very little is known about whether the reinitiation competence of post-termination ribosomes is also subjected to regulation.

A growing body of evidence suggests that reinitiation relies on certain initiation factors (eIFs) that remain attached to the post-termination ribosomes[4]. One such factor is eukaryotic initiation factor 3 (eIF3), which has been shown to ensure prolonged retention of post-termination ribosomes on mRNA[12,13]. The crucial role of eIF3 in translation reinitiation has been demonstrated in yeast[13], plant[14] and mammalian cells[15]. As the largest and most complex initiation factor, eIF3 is a multisubunit complex that binds to the solvent-exposed side of the 40S subunit[16,17]. Besides a general role in translation initiation, eIF3 has been reported to regulate protein synthesis in a mRNA-specific manner[18]. Structural studies of eIF3 in the context of the 43S preinitiation complex revealed that one 'arm' of eIF3 extends to the intersubunit surface[19,20]. Rearrangement of eIF3 is expected to occur upon the 60S subunit joining at the start codon, which probably explains the detachment of eIF3 from the 80S ribosome. Using selective profiling of scanning ribosomes, several recent studies have reported that eIF3 could linger on the 80S ribosome during the early stage of elongation[21–23]. This observation is in line with the proposal that the 80S-retained eIF3 makes the ribosome competent for reinitiation by stabilizing mRNA association and providing a platform to re-recruit other eIFs. How eIF3 remains attached to the elongating ribosomes and its role in subsequent translation reinitiation is of considerable interest.

The post-translational modification of proteins enables cells to respond swiftly to external and internal cues through dynamic regulation of protein function. *O*-GlcNAcylation is a noncanonical glycosylation that involves the attachment of single *O*-linked N-acetylglucosamine (*O*-GlcNAc) moieties to serine and threonine

Division of Nutritional Sciences, Cornell University, Ithaca, NY, USA. ✉e-mail: sq38@cornell.edu

residues of intracellular proteins[24,25]. Notably, *O*-GlcNAc signaling is highly sensitive to various forms of cellular stress, including nutrient starvation[26]. As a result, *O*-GlcNAcylation has been proposed to act as a nutrient sensor that regulates cellular processes including transcription, translation, signal transduction and metabolism[27]. Interestingly, many eIFs undergo *O*-GlcNAc modification either constitutively or in a stress-inducible manner[28]. We previously reported that heat shock stress triggers eIF4G1 *O*-GlcNAcylation, thereby promoting selective translation of heat shock proteins[29]. Very little is known about whether and how *O*-GlcNAc signaling affects translational regulation in response to nutrient starvation.

Here, using eIF3-coupled ribosome profiling, we found that amino acid starvation triggers prolonged eIF3–80S association, which subsequently promotes translation reinitiation. We discovered that dynamic modification of eIF3a in the form of *O*-GlcNAc controls eIF3–80S interaction. Whereas constitutive *O*-GlcNAcylation of eIF3a facilitates eIF3 recycling from 80S ribosomes, stress-induced de-*O*-GlcNAcylation promotes eIF3 retention on elongating ribosomes. This finding suggests an unexpected structural remodeling of eIF3 and highlights *O*-GlcNAc modification as a toggle switch between initiation and reinitiation events.

## Results

**Amino acid starvation prolongs eIF3–80S association.** We first examined whether eIF3–80S association is responsive to amino acid deprivation, a potent inducer of integrates stress response. We separated ribosomes from the whole-cell lysates of mouse embryonic fibroblasts (MEFs) via a sucrose cushion (Fig. 1a). After 2 h of amino acid starvation, a substantial amount of eIF3a was relocated from the soluble fraction to the ribosome pellet. This is further corroborated by the distribution of eIF3a in polysome fractions despite the starvation-induced polysome disassembly (Extended Data Fig. 1a). Because mRNAs like *Atf4* are under selective translation in response to amino acid shortage, we quantified eIF3-associated messengers by immunoprecipitation (IP) of eIF3a followed by quantitative PCR with reverse transcription (RT–qPCR) (Fig. 1b). With comparable levels of total mRNA, a greater amount of *Atf4* transcript, but not the *Actb* control, was engaged with eIF3 under amino acid restriction.

To determine the position of eIF3–80S complexes across the transcriptome, we conducted eIF3-associated ribosome profiling (eIF3-seq) in MEFs with or without amino acid starvation (Fig. 1c). Unlike the previously reported translation complex profile sequencing (TCP-seq)[30], we enriched endogenous eIF3–80S complexes using eIF3a IP. Without crosslinking and 40S separation, this approach does not capture footprints derived from scanning ribosomes. As expected, eIF3–80S footprints were largely enriched at the start codon. In agreement with previous reports[22,23], a substantial number of eIF3–80S reads were also recovered from CDS (Fig. 1c). Unlike standard ribosome profiling (Ribo-seq) that shows evident three-nucleotide periodicity of footprints, eIF3-seq uncovered ribosome footprints with poor phasing. It is likely that the presence of eIF3 either changes the ribosome conformation or affects the 5′-end accuracy of nuclease digestion. This feature also ruled out the possibility that free eIF3 molecules reassociate with 80S ribosomes in the lysates. Further, not all the transcripts were equally engaged with eIF3–80S complexes in the CDS under normal growth conditions. Relative to the total 80S occupancy, we observed qualitative and quantitative differences in eIF3-associated elongating ribosomes on individual transcripts (Extended Data Fig. 1b). Intriguingly, many stress genes tend to retain eIF3 in the CDS of their transcripts, as revealed by gene ontology (GO) analysis (Extended Data Fig. 1b).

Upon amino acid deprivation, Ribo-seq showed decreased ribosome density at the start codon (Fig. 1d, upper). Strikingly, eIF3-seq revealed an elevated eIF3–80S peak at the start codon in comparison with the nutrient-rich control (Fig. 1d, lower). The accumulation of eIF3–80S complexes extended into CDS with greater enrichment within the first 150 nucleotides under nutrient starvation. Notably, starvation-induced eIF3 retention on 80S occurred on the majority of individual transcripts (Fig. 1e). As a result, the eIF3-associated transcripts were no longer limited to stress genes (Extended Data Fig. 1c). These results indicate that nutrient stress promotes eIF3 retention on elongating 80S ribosomes, forming prolonged eIF3–80S complexes.

**Amino acid starvation triggers de-*O*-GlcNAcylation of eIF3a.** It is unclear how amino acid deprivation leads to eIF3 retention on elongating ribosomes. Because eIF2α phosphorylation by GCN2 kinase is a common feature of nutrient starvation[11], we searched for potential targets using quantitative phosphoproteomics (Extended Data Fig. 2a). Among differential phosphopeptides, eIF2α and several metabolic enzymes were highly phosphorylated under amino acid restriction, as expected (Extended Data Fig. 2b and Supplementary Table 1). However, we identified very few proteins directly involved in translation. Intriguingly, lectin, one of the most abundant phosphoproteins in cells, showed a fivefold reduction in phosphorylation in starved cells (Extended Data Fig. 2c). Lectins are carbohydrate-binding proteins and whose phosphorylation has been implicated in *O*-GlcNAc signaling[31], which acts as a nutrient sensor that regulates a wide range of cellular processes, including translation[27]. This finding prompted us to survey proteins subjected to *O*-GlcNAc modification before and after amino acid starvation. To this end, we employed quantitative proteomics using stable isotope labeling by amino acids in cell culture (SILAC) (Fig. 2a). Differentially labeled MEFs were subjected to starvation ('heavy') or control ('light') followed by *O*-GlcNAc enrichment using the RL2 antibody[29]. A handful of translation initiation factors were enriched as *O*-GlcNAc species (Supplementary Table 2). Among them, eIF3a exhibited a twofold decrease in response to amino acid limitation (Fig. 2a, right). We confirmed this finding using agarose-bound wheatgerm agglutinin (WGA), which pulls down much less eIF3a under amino acid restriction (Fig. 2b). To directly demonstrate the *O*-GlcNAc modification of eIF3a, we incubated cells with azide-modified glucosamine followed by a click chemical reaction. eIF3a was readily pulled down by biotin from denatured whole-cell lysates, offering a direct evidence supporting *O*-GlcNAcylation of eIF3a (Fig. 2c).

As a noncanonical glycosylation, reversible *O*-GlcNAcylation is mediated by a sole pair of enzymes: *O*-GlcNAc transferase (OGT) and *O*-GlcNAcase (OGA)[24,25]. Whereas OGT catalyzes the transfer of a GlcNAc moiety from the donor substrate UDP–GlcNAc to the hydroxyl groups of Ser and Thr residues, OGA mediates the hydrolysis of this sugar modification. As an independent validation, we took advantage of a MEF cell line carrying the *Ogt* gene that can be deleted by simple administration of 4-hydroxytamoxifen (4-OHT)[29,32]. OGT depletion via 4-OHT pretreatment led to a marked reduction in total *O*-GlcNAc signals (Extended Data Fig. 2d). Likewise, eIF3a-associated *O*-GlcNAc signals were also decreased as manifested by pulldown assays using RL2 (Fig. 2d) or WGA (Extended Data Fig. 2e). Reciprocal IP further confirmed the dynamic *O*-GlcNAcylation of eIF3a before and after amino acid deprivation (Fig. 2e). The OGT-dependent eIF3a modification also holds true in HEK293 cells as RNA interference-mediated OGT knockdown clearly dampened *O*-GlcNAc signals of eIF3a (Extended Data Fig. 2f). To substantiate this finding further, we treated MEFs with Thiamet G, a potent OGA inhibitor (Extended Data Fig. 2g), and observed sustained *O*-GlcNAc signals of eIF3a even under amino acid restriction (Fig. 2f). These results collectively indicate that deprivation of amino acids triggers de-*O*-GlcNAcylation of eIF3a. Because *O*-GlcNAc biogenesis depends on the continuous supply of certain amino acids, it is conceivable that *O*-GlcNAcylation of eIF3a serves as a sentinel of intracellular nutrient status.

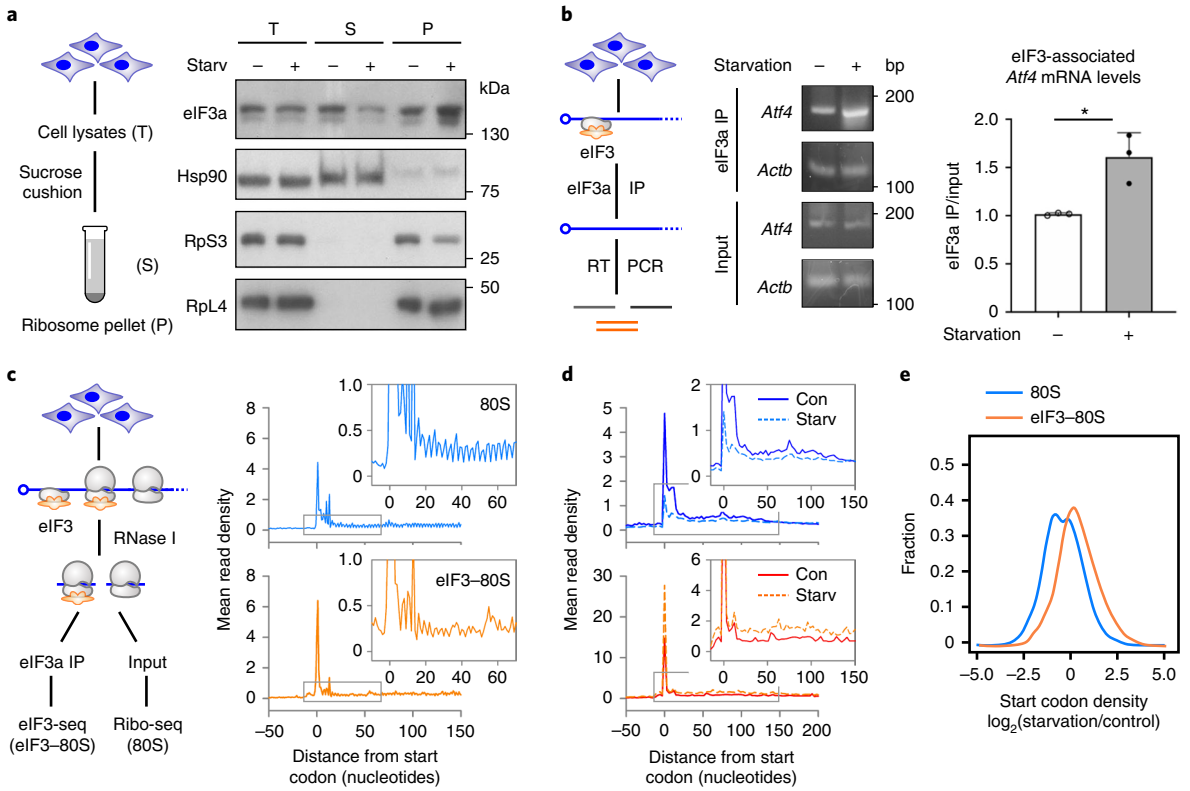


**Fig. 1 | Prolonged eIF3–80S association in response to amino acid starvation. a**, MEFs were treated with (+) or without (–) amino acid starvation for 2 h followed by a sucrose cushion. Whole-cell lysates (T), ribosome pellets (P) and supernatants (S) were immunoblotted using the antibodies indicated. Representative results of three independent experiments are shown. **b**, MEFs with (+) or without (–) amino acid starvation for 2 h were subjected to IP using eIF3a antibody. Total RNAs and eIF3-associated RNAs were extracted followed by RT–qPCR measuring *Actb* and *Aft4* mRNA levels. Relative *Atf4*/*Actb* ratios were normalized to the corresponding input. Error bars, mean ± s.d.; $^*P = 0.028$; two-way ANOVA; $n = 3$ independent experiments. **c**, The left-hand panel shows the schematic of eIF3-seq and Ribo-seq. The right-hand panels show metagene analysis of 80S (blue line) and eIF3–80S (orange line) footprints on transcripts aligned to start codons. The inserts show the three-nucleotide periodicity. **d**, Metagene analysis of 80S (blue line) and eIF3–80S (orange line) footprints on transcripts aligned to start codons. MEFs were subject to amino acid starvation for 2 h. The read density based on the codon was used for the aggregation plots. Inserts show the differential read density in CDS before and after starvation. **e**, Cumulative distribution of starvation-induced changes in read density at start codons for 80S (blue line) and eIF3–80S (orange line) footprints.

**Constitutive *O*-GlcNAcylation of eIF3a inhibits reinitiation.** It is unclear whether starvation-induced removal of *O*-GlcNAc from eIF3a promotes translation reinitiation via prolonged eIF3–80S association. If so, sustained *O*-GlcNAcylation on eIF3a would inhibit selective translation of ATF4. This was indeed the case. Constitutive *O*-GlcNAcylation of eIF3a by Thiamet G treatment for 16 h not only reduced the amount of *Atf4* mRNA associated with eIF3 (Fig. 3a), but also substantially attenuated ATF4 translation in response to starvation (Fig. 3b). Notably, neither the eIF2α signaling pathway nor *Atf4* transcription was altered by Thiamet G treatment (Extended Data Fig. 3a). The suppressed *Atf4* translation by Thiamet G was further confirmed by the firefly luciferase (Fluc) reporter assay (Fig. 3c). In addition, even 1 h treatment with Thiamet G is sufficient to reduce eIF3–*Atf4* interaction as well as ATF4 translation (Extended Data Fig. 3b–d). In line with the disrupted eIF3–80S association, Thiamet G treatment largely diminished the polysome-associated eIF3a especially upon amino acid deprivation (Extended Data Fig. 3e,f). eIF3-seq revealed that stress genes were no longer enriched among the eIF3-enriched transcripts before and after nutrient starvation (Extended Data Fig. 4a–c). Consistent with the deficient translation reinitiation in the presence of Thiamet G, Ribo-seq revealed very few reads from the main CDS of *Atf4*, even after 2 h of amino acid deprivation (Extended Data Fig. 4d). Therefore, hyper *O*-GlcNAcylation of eIF3a counteracts translation reinitiation by preventing eIF3 association with elongating ribosomes.

**Deficient *O*-GlcNAcylation promotes eIF3–80S association.** To fully investigate how dynamic *O*-GlcNAc modification regulates translation reinitiation, we examined the translational status in conditional *Ogt* null cells. Because prolonged OGT depletion is lethal, we limited the 4-OHT treatment to 24 h. Despite the increased association of *Atf4* mRNA with eIF3 (Extended Data Fig. 5a), ATF4 protein levels were minimally induced in starved cells lacking OGT (Extended Data Fig. 5b). The attenuated ATF4 translation in cells lacking OGT is probably due to cellular toxicity[29]. Indeed, *Ogt* null cells showed evident polysome disassembly (Extended Data Fig. 5c) and reduced global protein synthesis as measured by puromycin labeling (Extended Data Fig. 5d). We reasoned that when eIF3a is void of *O*-GlcNAcylation, the prolonged eIF3–80S association could lead to eIF3 sequestration. Indeed, *Ogt* null cells showed a greater amount of eIF3a in polysome fractions than the wild-type (Extended Data Fig. 5c). Some other eIF3 subunits such as eIF3c and eIF3g showed a similar pattern as eIF3a (Extended Data Fig. 5e). As an independent validation, we applied SILAC to conditional *Ogt* null cells to quantify ribosomal proteins associated with eIF3a with or without *O*-GlcNAc modification (Fig. 3d, Supplementary Table 3). From two independent replicates by

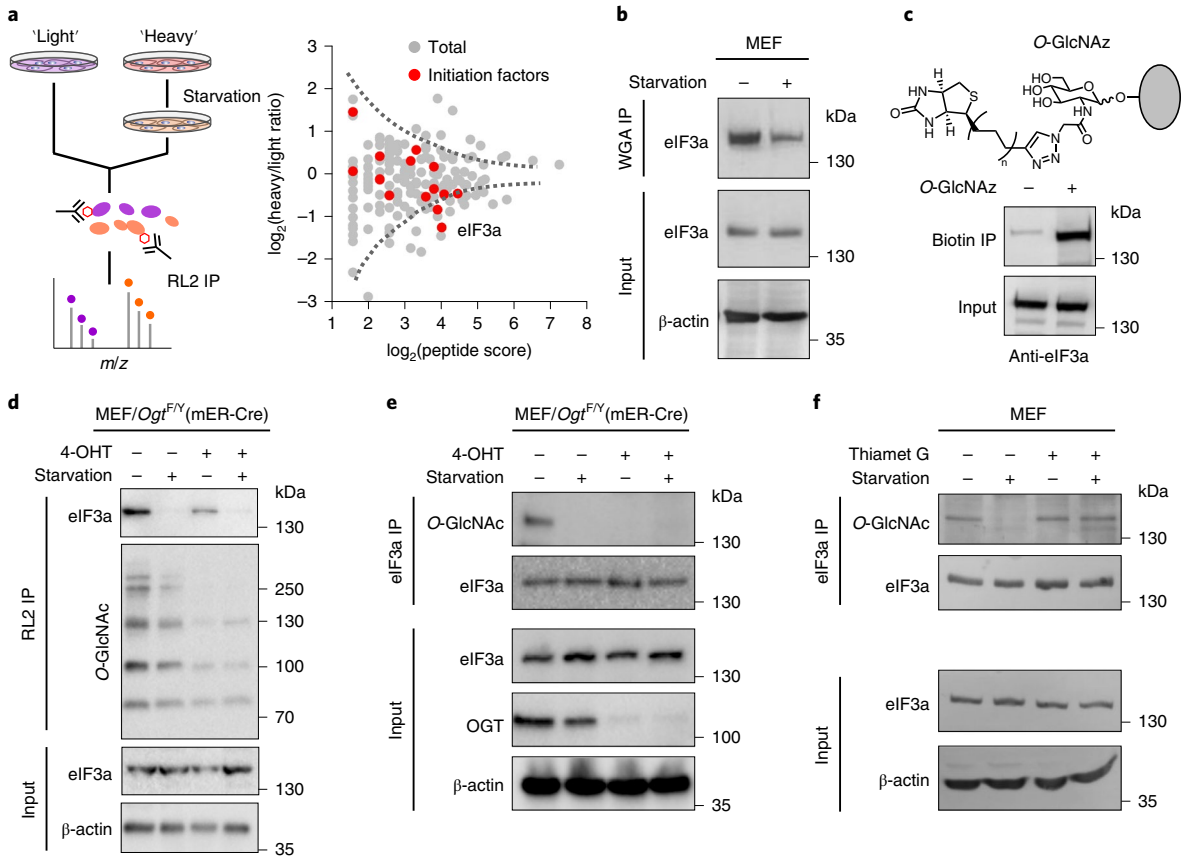


**Fig. 2 | Amino acid starvation triggers de-*O*-GlcNAcylation of eIF3a. a**, MEFs were cultured in 'light' or 'heavy' media for five passages followed by amino acid starvation for 2 h. *O*-GlcNAcylated species were purified using IP by the *O*-GlcNAc antibody RL2 followed by MS. The right-hand panel shows a scatterplot of *O*-GlcNAcylated proteins before and after amino acid starvation. The original peptide score ($log_2$) and starvation-induced fold changes are shown in the *x* and *y* axis, respectively. Initiation factors are colored red with eIF3a highlighted. **b**, MEFs with (+) or without (−) amino acid starvation for 2 h were subjected to IP using WGA antibody followed by immunoblotting. Representative results of three independent experiments are shown. **c**, MEFs treated with (+) or without (−) azide-modified glucosamine for 48 h were subjected to 'click chemistry' followed by IP using streptavidin beads and immunoblotting. Representative results of three independent experiments are shown. **d**, MEF/*Ogt* $^{F/Y}$(mER-Cre) cells were pretreated with (+) or without (−) 0.5 μM 4-OHT for 24 h followed by normal media for another 24 h. Cells were then subjected to amino acid starvation for 2 h before IP using the RL2 antibody followed by immunoblotting. Representative results of three independent experiments are shown. **e**, MEFs as in **d** were subjected to IP using the eIF3a antibody followed by immunoblotting. Representative results of three independent experiments are shown. **f**, MEFs were treated with 0.1 μM Thiamet G for 16 h followed by amino acid starvation for 2 h. Whole-cell lysates were immunoprecipitated using the eIF3a antibody followed by immunoblotting. Representative results of three independent experiments are shown.

isotope switching, more 60S ribosomal proteins were recovered from eIF3 in cells lacking OGT (Fig. 3d, right). By contrast, the binding of 40S subunit to eIF3 remains constant regardless of the modification. These results support the retention of eIF3 on 80S elongating ribosomes in cells lacking OGT.

We next examined the status of eIF3–80S association in cells lacking OGT. In agreement with the reduced protein synthesis, Ribo-seq showed decreased 80S footprints in CDS after 4-OHT treatment (Fig. 3e). Remarkably, OGT knockout led to an evident increase in eIF3–80S footprints in CDS even under the normal growth condition (Fig. 3e). Because few GO categories were overrepresented in eIF3-enriched transcripts (Extended Data Fig. 6a and b), the increased eIF3–80S association in the absence of OGT is probably global. A direct comparison of ribosome density between OGT depletion and amino acid starvation revealed a positive correlation (Extended Data Fig. 6c, Spearman's $Rho = 0.81$), suggesting that lack of OGT mimics the starvation-induced de-*O*-GlcNAcylation. Supporting this notion, a substantial number of footprints were uncovered from the main CDS of *Atf4* even under the nutrient-rich condition (Fig. 3f). Upon amino acid deprivation, the maintained ribosome occupancy across the *Atf4* CDS is in accordance with the enhanced reinitiation under hypo-*O*-GlcNAcylation. However, under global translation inhibition in the absence of OGT (Extended Data Fig. 5c), the output of ATF4 translation is severely compromised. It is noteworthy that OGT depletion together with amino acid limitation led to an increased ribosome density in the 3′ untranslated region (3′-UTR) (Extended Data Fig. 6d), echoing the uncontrolled translation reinitiation due to prolonged eIF3–80S association.

**Characterization of eIF3a *O*-GlcNAcylation.** To understand how *O*-GlcNAcylation of eIF3a regulates eIF3–80S association, it is important to determine the modification sites. We purified endogenous eIF3a from HEK293 cells and applied tandem mass spectrometry (MS/MS) to map the positions of *O*-GlcNAc modification. With a peptide coverage of 88%, mass spectrometry (MS) revealed only two modification sites with high confidence (Ser225 and Thr336) (Fig. 4a and Supplementary Table 4). To confirm the identified modification sites, we cloned the full-length eIF3a and fused green fluorescent protein (GFP) to the N terminus to increase

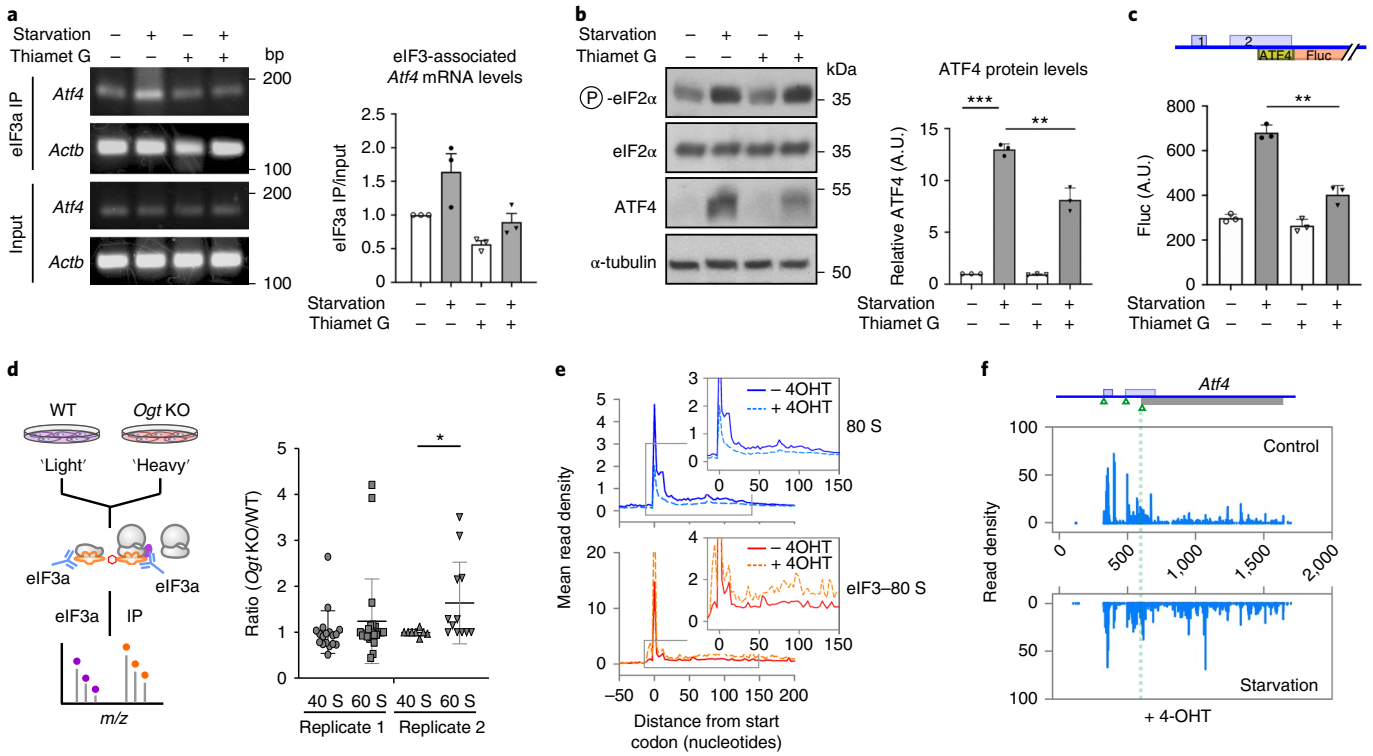


**Fig. 3 | Dynamic *O*-GlcNAcylation of eIF3a regulates translation reinitiation. a**, MEFs were treated with 0.1 μM Thiamet G for 16 h followed by amino acid starvation for 2 h. Whole-cell lysates were immunoprecipitated using the eIF3a antibody. Total RNAs and eIF3-associated RNAs were extracted followed by RT–PCR measuring *Actb* and *Aft4* mRNA levels. Relative *Atf4*/*Actb* ratios were normalized to the corresponding input. Error bars, mean ± s.d.; $^{*}P = 0.034$; two-way ANOVA; $n = 3$ independent experiments. **b**, MEFs as in **a** were subjected to immunoblotting using the antibodies indicated. The right-hand panel shows the relative ATF4 protein levels normalized to α-tubulin. Error bars, mean ± s.d.; $^{**}P = 0.0083$; $^{***}P = 0.00066$; two-way ANOVA; $n = 3$ independent experiments. **c**, MEFs as in **a** were transfected with ATF4–Fluc reporter plasmids. After amino acid starvation for 2 h, Fluc activities were measured by luminometry. Error bars, mean ± s.d.; $^{**}P = 0.0057$; two-way ANOVA; $n = 3$ biological replicates. **d**, MEF/*Ogt*$^{F/Y}$(mER-Cre) cells were cultured in 'light' or 'heavy' media for five passages before treating 'heavy' cells with 4-OHT to silence *Ogt*. Proteins were immunoprecipitated using an eIF3a antibody followed by MS. The right-hand panel shows the relative ratio of eIF3a-associated 60S and 40S ribosomal proteins in MEFs with or without 4-OHT treatment. Two biological replicates are shown. Error bars, mean ± s.d.; $^{*}P = 0.0496$; two-way ANOVA. **e**, MEFs as in **d** were subjected to eIF3-seq and Ribo-seq followed by metagene analysis of 80S (blue line) and eIF3–80S (orange line) footprints on transcripts aligned to start codons. The read density based on the codon was used for the aggregation plots. Inserts show the differential read density in CDS with or without *Ogt* silencing. **f**, Distribution of 80S footprints in the *Atf4* transcript from MEFs *Ogt* knockout (KO) before and after amino acid starvation. A.U., arbitrary unit.

the expression level in transfected cells. The transgene GFP–3A preserved *O*-GlcNAc modification and responded well to nutrient starvation (Extended Data Fig. 7a). Additionally, GFP–eIF3a showed similar distribution as the endogenous eIF3a in ribosome fractions separated by sucrose gradient (Extended Data Fig. 7a). Introducing S225A and T336A double mutation (STA) eliminated *O*-GlcNAc signals from purified GFP–3A fusion proteins (Fig. 4b). Intriguingly, a greater amount of large ribosomal subunit RPL4 was coprecipitated with the STA mutant than the wild-type. This result provides independent evidence that the lack of *O*-GlcNAc modification on eIF3a promotes eIF3–80S interaction. To probe the modification sites in more detail, we introduced a single T336A mutation into GFP–3A but only found a slight decrease in *O*-GlcNAc signals (Extended Data Fig. 7b). We next created a S225 deletion mutant that showed an almost complete loss of *O*-GlcNAc signals from eIF3a (Fig. 4c), indicating that S225 is the major modification site of eIF3a. Like the STA mutant, the ΔS225 mutant pulled down more RPL4 molecules than the wild-type. Therefore, the site-specific *O*-GlcNAc mark on eIF3a serves as a molecular switch in controlling eIF3–80S complex formation.

**Deficient *O*-GlcNAcylation of eIF3a drives ATF4 reinitiation.** OGT is responsible for the *O*-GlcNAc modification of hundreds of proteins. To dissect the specific effect of eIF3a *O*-GlcNAcylation without *Ogt* silencing, it is highly desirable to create cell lines harboring endogenous eIF3a that cannot be modified by *O*-GlcNAc. We genetically engineered the endogenous *Eif3a* in HEK293 cells via CRISPR–Cas9 gene editing using single guide RNAs targeting S225. As expected, most resultant cells had an insert/deletion at the *Eif3a* locus, giving rise to nonfunctional eIF3a. Nearly all the surviving cells also had full-length eIF3a, arguing for its essential role in cell viability. From hundreds of cell clones, we selected a cell line harboring a S225G mutation at one locus of eIF3a (Fig. 4d). Because of the presence of wild-type eIF3a, the mutant cell line had marginally reduced global protein synthesis (Extended Data Fig. 7c), and a slightly decreased growth rate (Extended Data Fig. 7d). With comparable total eIF3a protein levels, we observed an approximate 50% reduction in *O*-GlcNAc signals associated with eIF3a (Fig. 4d, right panel). This result confirmed that S225 is the major modification site on eIF3a, if not the only one. Remarkably, the S225G mutant cells exhibited a more robust amino acid response than wild-type cells by inducing higher ATF4 protein levels upon amino acid deprivation (Fig. 4e). In fact, longer exposure of the western blots revealed higher basal levels of ATF4 even before nutrient starvation. This was not due to altered *Atf4* mRNA levels in these cells (Extended Data Fig. 7e). Rather, this result is a strong indication of

enhanced translation reinitiation under lowered *O*-GlcNAcylation of eIF3a. In agreement with this notion, ATF4 reporter assays also showed higher Fluc levels in S225G mutant cells than wild-type cells with or without nutrient starvation (Fig. 4f).

**Deficient *O*-GlcNAcylation affects translation reinitiation.** The ATF4 transcript contains two short uORFs in the 5′-UTR: uORF1 near the 5′ terminus and uORF2 overlapping with the main CDS but in different reading frames. The uORF1 permits reinitiation when the terminating ribosome remains on the messenger together with eIF3. Using ATF4–Fluc reporters[33], we confirmed that deletion of uORF1 abolished the starvation-induced ATF4 translation (Extended Data Fig. 8a). Consistently, lack of uORF1 reduced eIF3a interaction with *Atf4* mRNA (Extended Data Fig. 8b). Interestingly, in HEK293 cells bearing the eIF3a(S225G) mutant, the eIF3a–*Atf4* interaction was restored despite the lack of uORF1 (Extended Data Fig. 8c). This result confirms the crucial role of *O*-GlcNAcylation of eIF3a in controlling eIF3–80S association.

*Atf4* is not the only transcript capable of translation reinitiation. A recent study reported that many oncogenes undergo translation reinitiation in a density-regulated protein (DENR)-dependent manner[34]. We selected a transcript encoding mitogen-activated protein kinase kinase 6 (MAP2K6) that is subjected to translation reinitiation. Like ATF4, the MAP2K6 protein level was markedly increased upon amino acid starvation (Fig. 5a). We also confirmed starvation-induced eIF3 interaction with the *Map2k6* mRNA (Extended Data Fig. 8d). This was not due to changes in mRNA abundancy because the steady-state *Map2k6* levels were comparable before and after starvation (Extended Data Fig. 8e). In HEK293 cells bearing the eIF3a(S225G) mutant, MAP2K6 expression was constitutively elevated in a manner similar to ATF4 (Fig. 5a), suggesting that the crucial role of *O*-GlcNAcylation of eIF3a in translation reinitiation is not limited to ATF4. Because translation reinitiation relies on uORF, we created an artificial mRNA reporter bearing a uORF encoding SIINFEKL followed by nano-luciferase HiBiT (Fig. 5b). This construct also responds to amino acid starvation, confirming its reinitiation feature. Once again, eIF3a(S225G) mutation promoted reinitiation of the uORF reporter as evidenced by the sustained HiBiT signals (Fig. 5b). We conclude that dynamic *O*-GlcNAcylation of eIF3a fine-tunes the translational output by

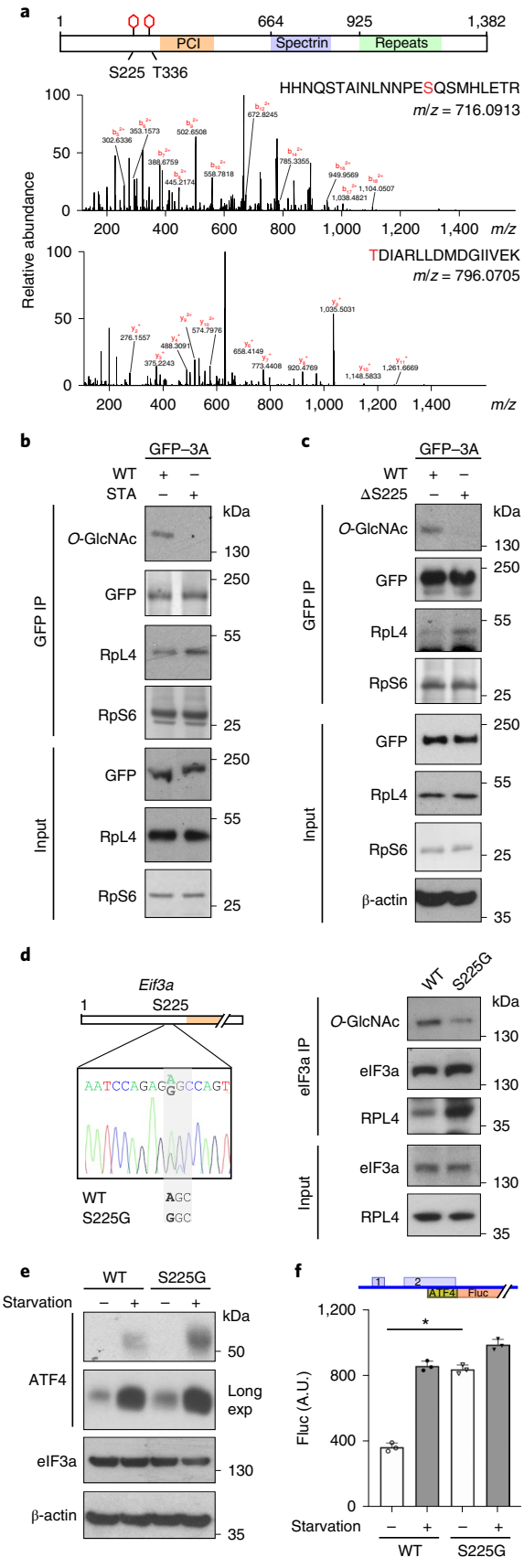


**Fig. 4 | Deficient *O*-GlcNAcylation of eIF3a promotes eIF3–80S association. a**, Cell lysates from HEK293 cells were immunoprecipitated with eIF3a antibody followed by MS. Electron transfer/higher energy collision dissociation MS/MS spectrum of *m/z* 587.79132+ identified *O*-GlcNAcylation at S225 and T336 (red), illustrated along the peptide sequences shown. HexNAc, *N*-acetylhexoseamine. **b**, HEK293 cells were transfected with plasmids expressing EGFP-tagged eIF3A wild-type (WT) or a double mutant (STA) for 24 h. Transfected cells were immunoprecipitated using an anti-GFP antibody followed by immunoblotting. The lower panel shows the quantification of relative binding of the STA mutant to ribosomal subunits. Representative results of three independent experiments are shown. **c**, HEK293 cells were transfected with plasmids expressing EGFP-tagged eIF3A WT or a deletion mutant (ΔS225) for 24 h. Transfected cells were immunoprecipitated using an anti-GFP antibody followed by immunoblotting. The lower panel shows the quantification of relative binding of the ΔS225 mutant to ribosomal subunits. Representative results of three independent experiments are shown. **d**, Genome editing using CRISPR–Cas9 resulted in S225G mutation in HEK293 cells with the DNA sequencing result highlighted in the left-hand panel. The right-hand panel shows the IP of eIF3a WT or S225G mutant from HEK293 cells using an eIF3a antibody followed by immunoblotting. Representative results of three independent experiments are shown. **e**, Cells as in **d** were subjected to immunoblotting using the antibodies indicated. **f**, Cells as in **d** were transfected with ATF4–Fluc reporter plasmids. After amino acid starvation for 2 h, Fluc activities were measured by luminometry. Error bars, mean ± s.d.; **P* = 0.034; two-way ANOVA; *n* = 3 biological replicates.

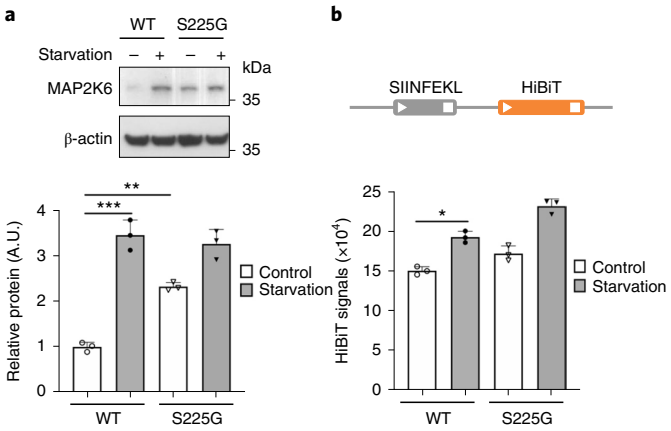


**Fig. 5 | Deficient *O*-GlcNAcylation of eIF3a affects general translation reinitiation. a**, HEK293 cells with or without eIF3a(S225G) mutation were subjected to immunoblotting using antibodies indicated. The lower panel shows the relative MAP2K6 protein levels normalized to β-actin. Error bars, mean ± s.d.; $^{**}P=0.0072$; two-way ANOVA; $n=3$ independent experiments. **b**, HEK293 cells with or without eIF3a(S225G) mutation were subjected to amino acid starvation for 2 h followed by transfection of uORF reporter. HiBiT signals were measured by luminometry. Error bars, mean ± s.d.; $^{*}P=0.042$; two-way ANOVA; $n=3$ biological replicates.

controlling eIF3–80S association, thereby balancing eIF3 recycling and translation reinitiation (Fig. 6).

## Discussion

Approximately 50% of mammalian transcripts contain at least one uORF[35], whose translation has been implicated in development as well as the stress response. In addition to the translational products of uORF, uORF translation per se can regulate the translation potential of the downstream ORF[36]. By sequestering ribosomes, most uORFs negatively regulate translation of the main CDS. Interestingly, uORFs could also positively regulate the downstream CDS via reinitiation, a mechanism exploited by stress genes whose expression is upregulated upon specific internal and external signals[4]. One fundamental question is how the terminating ribosome regains the scanning capability on those transcripts. We found that dynamic *O*-GlcNAcylation of eIF3a controls translation reinitiation in mammalian cells by coordinating eIF3–80S association in a stress-dependent manner.

The transient nature of eIF3–80S interaction suggests the inherent instability of eIF3 association in the presence of the 60S subunit. Mammalian eIF3 contains 13 subunits, forming an octameric proteasome, COP9, eIF3/Mpr1–Pad1 N-terminal (PCI/MPN) core and a peripheral module[17]. The entire eIF3 complex bestrides the solvent-exposed surface of the 40S by spanning entry and exit ends of the mRNA channel[19]. It is possible that *O*-GlcNAcylation at eIF3a modulates the overall structure of the whole eIF3 complex, triggering eIF3 dissociation from the 40S upon 60S joining. This is in accordance with the proposed role for eIF3 in 60S subunit recycling by preventing ribosomal subunit reassociation after termination[37]. From the cryogenic electron microscopy structures of mammalian eIF3, the S225 residue of eIF3a is located at the helical bundle next to the insert connecting eIF3a and eIF3c (Extended Data Fig. 9). How this single-site modification triggers conformational change in eIF3 merits further investigation. Notably, the PCI/MPN octamer core of eIF3 has topological similarity with the proteasome lid and the COP9 signalosome. Because the Rpt2 ATPase in the mammalian proteasome 19S cap is also modified by *O*-GlcNAc[38], the substrate specificity of OGT is probably based on the similar structural basis. Future efforts in solving structures of eIF3–80S complexes may shed light on the regulatory mechanism of *O*-GlcNAc modification.

It is noteworthy that, whereas *O*-GlcNAc modification occurs pervasively in eukaryotic cells, the budding yeast *Saccharomyces cerevisiae* lacks both OGT and OGA genes. Although yeast and mammalian cells share many features in the operational mechanisms of reinitiation, they may utilize distinct strategies to modulate their reinitiation efficiencies. Interestingly, cauliflower mosaic virus relies on a viral transactivator protein together with the reinitiation supporter protein to retain eIF3 on the 80S ribosome[14,39]. Despite its crucial role in reinitiation, the prolonged eIF3–80S association comes at a cost under normal growth conditions. Genetic ablation of OGT severely inhibits protein synthesis, presumably by sequestrating eIF3 that becomes a limiting factor for general protein synthesis. Therefore, ribosome recycling and reinitiation need to be balanced to maintain intracellular homeostasis under

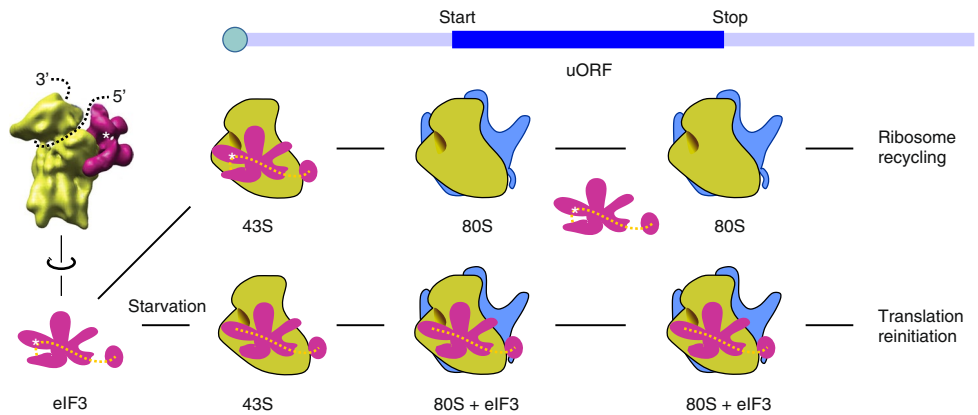


**Fig. 6 | A model of eIF3–80S association orchestrated by dynamic *O*-GlcNAcylation of eIF3a.** Under the normal growth condition, eIF3a, the core subunit of eIF3 (red), is modified by *O*-GlcNAc (white star) that does not affect 40S (yellow) association to form the 43S preinitiation complex. Following 60S (blue) joining, however, *O*-GlcNAcylated eIF3a destabilizes the eIF3–40S association, resulting in release of eIF3 from the elongating 80S ribosomes. In the absence of eIF3, the 80S ribosome is subjected to recycling at the stop codon. Following amino acid starvation, the de-*O*-GlcNAcylated eIF3a permits interaction between eukaryotic ribosomal protein L24 (eL24) and eIF3, thereby stabilizing eIF3–40S–60 complex formation. The eIF3–80S ribosome at the stop codon promotes translation reinitiation by maintaining mRNA binding and subsequent scanning. By coupling fluctuations in nutrient availability to translational reprogramming, dynamic *O*-GlcNAcylation of eIF3a represents an additional layer of integrated stress response.

normal and stress conditions. We propose that, whereas constitutive *O*-GlcNAcylation of eIF3a facilitates eIF3 recycling from 80S ribosomes, stress-induced de-*O*-GlcNAcylation promotes eIF3 retention on elongating ribosomes. Because *O*-GlcNAcylation is highly nutrient- and stress-sensitive[27,29], the dynamic *O*-GlcNAcylation of eIF3a potentially links stress-sensing and translational reprogramming in the integrated stress response.

## Online content

Any methods, additional references, Nature Research reporting summaries, source data, extended data, supplementary information, acknowledgements, peer review information; details of author contributions and competing interests; and statements of data and code availability are available at https://doi.org/10.1038/s41589-021-00913-4.

Received: 3 January 2021; Accepted: 29 September 2021;
Published online: 09 December 2021

## References

1. Hinnebusch, A. G. The scanning mechanism of eukaryotic translation initiation. *Annu. Rev. Biochem.* **83**, 779–812 (2014).
2. Jackson, R. J., Hellen, C. U. & Pestova, T. V. The mechanism of eukaryotic translation initiation and principles of its regulation. *Nat. Rev. Mol. Cell Biol.* **11**, 113–127 (2010).
3. Hershey, J. W. B., Sonenberg, N. & Mathews, M. B. Principles of translational control. *Cold Spring Harb. Perspect. Biol.* **11**, a032607 (2019).
4. Gunisova, S., Hronova, V., Mohammad, M. P., Hinnebusch, A. G. & Valasek, L. S. Please do not recycle! Translation reinitiation in microbes and higher eukaryotes. *FEMS Microbiol. Rev.* **42**, 165–192 (2018).
5. Hinnebusch, A. G. Translational regulation of GCN4 and the general amino acid control of yeast. *Annu. Rev. Microbiol.* **59**, 407–450 (2005).
6. Lu, P. D., Harding, H. P. & Ron, D. Translation reinitiation at alternative open reading frames regulates gene expression in an integrated stress response. *J. Cell Biol.* **167**, 27–33 (2004).
7. Vattem, K. M. & Wek, R. C. Reinitiation involving upstream ORFs regulates ATF4 mRNA translation in mammalian cells. *Proc. Natl Acad. Sci. USA* **101**, 11269–11274 (2004).
8. Kozak, M. Constraints on reinitiation of translation in mammals. *Nucleic Acids Res.* **29**, 5226–5232 (2001).
9. Luukkonen, B. G., Tan, W. & Schwartz, S. Efficiency of reinitiation of translation on human immunodeficiency virus type 1 mRNAs is determined by the length of the upstream open reading frame and by intercistronic distance. *J. Virol.* **69**, 4086–4094 (1995).
10. Kozak, M. Effects of intercistronic length on the efficiency of reinitiation by eucaryotic ribosomes. *Mol. Cell. Biol.* **7**, 3438–3445 (1987).
11. Wek, R. C., Jiang, H. Y. & Anthony, T. G. Coping with stress: eIF2 kinases and translational control. *Biochem. Soc. Trans.* **34**, 7–11 (2006).
12. Skabkin, M. A., Skabkina, O. V., Hellen, C. U. & Pestova, T. V. Reinitiation and other unconventional posttermination events during eukaryotic translation. *Mol. Cell.* **51**, 249–264 (2013).
13. Mohammad, M. P., Munzarova Pondelickova, V., Zeman, J., Gunisova, S. & Valasek, L. S. In vivo evidence that eIF3 stays bound to ribosomes elongating and terminating on short upstream ORFs to promote reinitiation. *Nucleic Acids Res.* **45**, 2658–2674 (2017).
14. Park, H. S., Himmelbach, A., Browning, K. S., Hohn, T. & Ryabova, L. A. A plant viral "reinitiation" factor interacts with the host translational machinery. *Cell* **106**, 723–733 (2001).
15. Hronova, V. et al. Does eIF3 promote reinitiation after translation of short upstream ORFs also in mammalian cells? *RNA Biol.* **14**, 1660–1667 (2017).
16. Hershey, J. W. The role of eIF3 and its individual subunits in cancer. *Biochim. Biophys. Acta* **1849**, 792–800 (2015).
17. Valasek, L. S. et al. Embraced by eIF3: structural and functional insights into the roles of eIF3 across the translation cycle. *Nucleic Acids Res.* **45**, 10948–10968 (2017).
18. Lee, A. S., Kranzusch, P. J. & Cate, J. H. eIF3 targets cell-proliferation messenger RNAs for translational activation or repression. *Nature* **522**, 111–114 (2015).
19. des Georges, A. et al. Structure of mammalian eIF3 in the context of the 43S preinitiation complex. *Nature* **525**, 491–495 (2015).
20. Siridechadilok, B., Fraser, C. S., Hall, R. J., Doudna, J. A. & Nogales, E. Structural roles for human translation factor eIF3 in initiation of protein synthesis. *Science* **310**, 1513–1515 (2005).
21. Wagner, S. et al. Selective translation complex profiling reveals staged initiation and co-translational assembly of initiation factor complexes. *Mol. Cell* **79**, 546–560 (2020).
22. Bohlen, J., Fenzl, K., Kramer, G., Bukau, B. & Teleman, A. A. Selective 40S footprinting reveals cap-tethered ribosome scanning in human cells. *Mol. Cell* **79**, 561–574 (2020).
23. Lin, Y. et al. eIF3 associates with 80S ribosomes to promote translation elongation, mitochondrial homeostasis, and muscle health. *Mol. Cell* **79**, 575–587 (2020).
24. Hart, G. W., Housley, M. P. & Slawson, C. Cycling of O-linked beta-N-acetylglucosamine on nucleocytoplasmic proteins. *Nature* **446**, 1017–1022 (2007).
25. Bond, M. R. & Hanover, J. A. A little sugar goes a long way: the cell biology of O-GlcNAc. *J. Cell Biol.* **208**, 869–880 (2015).
26. Martinez, M. R., Dias, T. B., Natov, P. S. & Zachara, N. E. Stress-induced O-GlcNAcylation: an adaptive process of injured cells. *Biochem. Soc. Trans.* **45**, 237–249 (2017).
27. Yang, X. & Qian, K. Protein O-GlcNAcylation: emerging mechanisms and functions. *Nat. Rev. Mol. Cell Biol.* **18**, 452–465 (2017).
28. Li, X. et al. O-GlcNAcylation of core components of the translation initiation machinery regulates protein synthesis. *Proc. Natl Acad. Sci. USA* **116**, 7857–7866 (2019).
29. Zhang, X., Shu, X. E. & Qian, S. B. O-GlcNAc modification of eIF4GI acts as a translational switch in heat shock response. *Nat. Chem. Biol.* **14**, 909–916 (2018).
30. Archer, S. K., Shirokikh, N. E., Beilharz, T. H. & Preiss, T. Dynamics of ribosome scanning and recycling revealed by translation complex profiling. *Nature* **535**, 570–574 (2016).
31. Xing, L., Li, J., Xu, Y., Xu, Z. & Chong, K. Phosphorylation modification of wheat lectin VER2 is associated with vernalization-induced O-GlcNAc signaling and intracellular motility. *PLoS ONE* **4**, e4854 (2009).
32. Kazemi, Z., Chang, H., Haserodt, S., McKen, C. & Zachara, N. E. O-linked beta-N-acetylglucosamine (O-GlcNAc) regulates stress-induced heat shock protein expression in a GSK-3beta-dependent manner. *J. Biol. Chem.* **285**, 39096–39107 (2010).
33. Zhou, J. et al. $N^6$-Methyladenosine guides mRNA alternative translation during integrated stress response. *Mol. Cell* **69**, 636–647 e7 (2018).
34. Bohlen, J. et al. DENR promotes translation reinitiation via ribosome recycling to drive expression of oncogenes including ATF4. *Nat. Commun.* **11**, 4676 (2020).
35. Calvo, S. E., Pagliarini, D. J. & Mootha, V. K. Upstream open reading frames cause widespread reduction of protein expression and are polymorphic among humans. *Proc. Natl Acad. Sci. USA* **106**, 7507–7512 (2009).
36. Orr, M. W., Mao, Y., Storz, G. & Qian, S. B. Alternative ORFs and small ORFs: shedding light on the dark proteome. *Nucleic Acids Res.* **48**, 1029–1042 (2020).
37. Pisarev, A. V., Hellen, C. U. & Pestova, T. V. Recycling of eukaryotic posttermination ribosomal complexes. *Cell* **131**, 286–299 (2007).
38. Zhang, F. et al. O-GlcNAc modification is an endogenous inhibitor of the proteasome. *Cell* **115**, 715–725 (2003).
39. Thiebeauld, O. et al. A new plant protein interacts with eIF3 and 60S to enhance virus-activated translation re-initiation. *EMBO J.* **28**, 3171–3184 (2009).

## Methods

**Cell lines and reagents.** $Ogt^{F/Y}$(mER-Cre) and $Ogt^{F/Y}$(GFP) MEFs were provided by N. E. Zachara (The Johns Hopkins University School of Medicine) and were maintained in DMEM with 10% FBS (Sigma Aldrich). For amino acid starvation treatment, MEFs were incubated in HBSS buffer (Lonza) with 10% dialyzed FBS. Samples were collected at the indicated time points. 4-Hydroxytamoxifen (H7904) and Thiamet G (SML0244) were purchased from Sigma. Anti-eIF3A (3411), anti-RPS6 (2217), anti-p-eIF2α Ser51 (3398), anti-eIF2α (9722), anti-MMK6/MAP2K6 (9264), anti-eIF3C (2068) and anti-ATF4 (11815) were purchased from Cell Signaling. Anti-*O*-GlcNAc (RL2, MA1-072) was purchased from ThermoFisher Scientific; anti-Puromycin (PMY-2A4) was purchased from Developmental Studies Hybridoma Bank; β-actin monoclonal antibody (F1804) was from Sigma; anti-OGT (11576-2-AP), anti-eIF3g (11165-1-AP) and anti-RPL4 (11302-1-AP) were from Proteintech; anti-GFP (NB600-308) was from Novus; and small interfering RNA targeting human OGT was purchased from Santa Cruz. WGA agarose beads were purchased from Vector Laboratories (AL-1023-2).

**Plasmid constructions.** eIF3a complementary DNA was cloned from plasmid containing complete human eIF3a cDNA (BC114429, Transomic) by PCR using primers 5′-GCCGGATATCCAATGCCGGCCTATTTTCAGAGG-3′ and 5′-GAATGCGGCCGCTTAACGTCGTACTGTGGTCC-3′. The amplified eIF3a coding sequences were inserted into enhanced green fluorescence protein (EGFP)-C1 (Clotech). eIF3a mutants were generated using the QuikChange II site-directed mutagenesis kit according to the manufacturer's instruction (Stratagene). The 5′-UTR of MAP2K6 was cloned from HeLa cell cDNA library using primers 5′-CCGGAAGCTTAGTTCCAAGTTTGGAGCTTTTAGC-3′ and 5′-CCGGCTGCAGGTCATGGTGGCCTTTCCTTTGATGGGGGAGGGGAG-3′. The 5′-UTR was then inserted into pGL3-Luciferase reporter using HindIII and PstI sites. Luciferase reporters (pGL3 TK-ATF4) bearing uORF1 or uORF2 start codon mutations were provided by R. C. Wek. In short, the AUG codons of uORF1 or uORF2 were mutated to AGG using a site-mutagenesis kit (Strategene). All plasmids were confirmed by DNA sequencing.

**uORF mRNA reporters.** To generate the uORF reporter encoding SIINFEKL and HiBiT before GFP, full-length GFP was amplified from pcDNA3–EGFP using 5′-CTCGAGCAGCTGGAATCGATCATCAACTTCGAAAAGCTATAGTGCA ATCCCCCAAAACAGACAGAGCCAGGATGGTGAGCAAGG-3′ and 5′-CAGACGTGTGCTCTTCCGATCT-3′. The resulting PCR product was reamplified using primer 5′- GTGAGCGGCTGGCGGCTGTTCAAGAAGATT AGCGCTCGAGATGGTGAGCAAGGGCGAGGA-3′ and 5′-TAATACGACT CACTATAGGGACATTTGCTTCTGACACAACATGGAATCGATCAT CAACTTCGAAAAGCTATAGAGCAACCTCAAACAAAAAAAAAAAG TGAGCGGCTGGCGG-3′. Two micrograms of the PCR product was subjected to in vitro transcription using T7 mMessage mMachine kit (Ambion) followed by poly(A) tailing kit (Ambion), according to the manufacturer's instructions. The final mRNA product was used for transfection.

**Generation of eIF3a mutant cell lines by LentiCRISPRv2.** LentiCRISPRv2 plasmid targeting eIF3a was constructed using previously described methods[40,41]. The single guide RNA sequence for eIF3a S225 is 5′-CACCGAGAGAGCCAGTC CATGCATT-3′ and 5′-AAACAATGCATGGACTGGCTCTCTC-3′. Lentiviral particles were packaged using Lenti-X 293 T cells (Clontech). Virus-containing supernatants were collected and filtered 48 h after transfection, and target cells were infected in the presence of 8 μg ml$^{-1}$ polybrene. To select stable cell lines, transfected cells were treated with 2 μg ml$^{-1}$ puromycin. Single cells grown on a 96-well plate were then expanded and analyzed by PCR amplification of genomic DNA flanking the CRISPR-targeted region. Forward primer for eIF3a S225: 5′-CTTTCAAATTCTGCCTCCAATAC-3′; reverse primer 5′-CTGCCACAATTCCATGCTGATAGC-3′. The editing of eIF3a was identified by DNA sequencing.

**Mass spectrometry to map the *O*-GlcNAcylation sites of eIF3a.** HEK293 cells were cultured in DMEM with 10% FBS until 80% confluency. Cell lysates were then collected for eIF3a IP. Purified eIF3a was submitted to the Proteomics Facility at Cornell University Institute of Biotechnology for MS as described previously[29]. Briefly, the 170-kDa protein bands from an SDS–polyacrylamide gel electrophoresis (SDS–PAGE) gel were subjected to in-gel digestion by trypsin followed by extraction of the digested peptide. Extracts from each sample were combined and lyophilized. The peptides were reconstituted in 20 μl of 0.5% formic acid for nano liquid chromatography tandem mass spectrometry (nanoLC-ESI-MS/MS) analysis using an Orbitrap Fusion Tribrid (ThermoFisher Scientific) mass spectrometer equipped with a nanospray Flex Ion Source coupled with a Dionex UltiMate3000RSLCnano system (Thermo). Peaks at 204.0867 Da (HexNAc oxonium ion) or 138.0545 Da (HexNAc fragment) were set as positive product identification. The SA energy was set at 20% and the electron-transfer dissociation (ETD) reaction time was set at 150 ms. Xcalibur 3.0 operation software and Orbitrap Fusion Tune Application v.2.1 (ThermoFisher Scientific) settings were used to gather data.

All MS and MS/MS raw spectra were searched against mouse protein database using Byonic v.2.8.2 (Protein Metrics). The glycan search was conducted using a list of 78 mammalian *O*-linked glycans. A maximum 2% false discovery rate (FDR) was applied to identify putative peptides.

**Immunoprecipitation.** Cells were washed twice with PBS buffer and lysed in ice-cold lysis buffer (10 mM HEPES, pH 7.4, 100 mM KCl, 5 mM $MgCl_2$, 100 μg ml$^{-1}$ of cycloheximide, 1% Triton X-100, proteinase inhibitor cocktail). Lysates were centrifuged at 16,000*g* for 15 min at 4 °C and supernatants were incubated with agarose beads coated with primary antibodies at 4 °C for overnight. Immunoprecipitants were washed at least three times with lysis buffer. The washed beads were resuspended in SDS–PAGE loading buffer (50 mM Tris, pH 6.8, 2% SDS, 10% glycerol, 1% β-mercaptoethanol, 0.005% bromophenol blue), denatured at 95 °C for 10 min and analyzed by immunoblotting.

**SILAC.** MEFs cultured in 'heavy' ($^{15}N$ and $^{13}C$) or 'light' ($^{14}N$ and $^{12}C$) isotope-containing medium for five passages before 'heavy' isotope labeled cells were treated with various conditions. Both cells were lysed in ice-cold lysis buffer, followed by centrifugation at 16,000*g* for 12 min at 4 °C. Equal amounts of supernatants were pooled and incubated with primary antibodies and agarose beads at 4 °C overnight. Immunoprecipitants were washed and resuspended in SDS–PAGE sample buffer. The protein content in the eluted material was resolved on an SDS–PAGE gel before band excision and in-gel trypsin digestion. The resultant peptide mixtures were pressure-loaded onto a C18 reverse-phase capillary column and analyzed by online nanoflow LC–MS/MS on an Agilent 1200 quaternary HPLC system (Agilent) connected to an LTQ-Orbitrap mass spectrometer (ThermoFisher Scientific) using a 2 h gradient. MS data were searched against human UniProt database using ProLuCID on IP2 (Integrated Proteomics Applications). Peptides were filtered using DTASelect2 with a 5 ppm D mass cutoff of the peptide masses and a false positive rate below 1%.

**Phosphoproteomics.** MEFs were lysed in ice-cold lysis buffer, followed by centrifugation at 16,000*g* for 12 min at 4 °C. Equal amount of soluble proteins was digested with trypsin. The resultant peptide mixtures were labeled using iTRAQ before pooled and enriched with phosphoprotein enrichment kit (Clotech). Phosphorylated peptides were pressure-loaded onto a C18 reverse-phase capillary column and analyzed by online nanoflow LC–MS/MS on an Agilent 1200 quaternary HPLC system (Agilent) connected to an LTQ-Orbitrap mass spectrometer (ThermoFisher Scientific) using a 2-h gradient. MS data were searched against human UniProt database with ProLuCID on IP2 (Integrated Proteomics Applications). Peptides were filtered using DTASelect2 with a 5 p.p.m. D mass cutoff of the peptide masses and a false positive rate below 1%.

**Metabolic labeling and detection of *O*-GlcNAcylation of eIF3a.** Metabolic labeling was performed using Click-iT azide-modified glucosamine metabolic glycoprotein labeling reagent (Invitrogen). Labeled proteins were extracted and biotinylated following manufacture's protocol (Click-iT protein analysis detection kit). Biotinylated proteins were purified by using streptavidin–agarose beads (Invitrogen), followed by immunoblotting analyses.

**RNA isolation and RT–qPCR.** Total RNA was extracted using TRIzol reagent (Invitrogen) according to the manufacturer's instruction. Single-strand cDNA synthesis was performed using the high-capacity cDNA reverse transcription kit (Applied Biosystems) followed by standard PCR reactions. Real-time quantitative PCR (qPCR) reactions were conducted on a LightCycler 480 using Power SYBR Green Master Mix (Applied Biosystems). Gene expression was normalized to *Actb* and calculated as a relative gene expression using the $2-\Delta\Delta Ct$ method. Oligonucleotide primers are as follows, mouse ATF4: forward 5′-CTTGATGTC CCCCTTCGACC-3′ and reverse 5′-CTTGTCGCTGGAGAACCCAT-3′; human ATF4: forward 5′-CCCTAGTCCAGGAGACTAATAAGCA-3′ and reverse 5′-ACTTTCTGGGAGATGGCCAAT-3′; mouse β-actin: forward 5′-TTGCTGACAGGATGCAGAAG-3′ and reverse 5′-ACTCCTGCTT GCTGATCCACAT-3′; human β-actin: forward 5′-AGCCTCGCCTTTGCC GA-3′ and reverse 5′-GCGCGGCGATATCATCATC-3′; human MAP2K6: forward 5′- TCAATGCTCTCGGTCAAGTG-3′ and reverse 5′- ATGCCCAGAC TCCAAATGTC-3′.

For eIF3a-associated mRNA IP, cells were washed twice with PBS and lysed in lysis buffer (10 mM HEPES, pH 7.4, 100 mM KCl, 5 mM $MgCl_2$, 100 μg ml$^{-1}$ of cycloheximide, 1% Triton X-100, proteinase inhibitor cocktail, 1 U SUPERase_In). Lysates were centrifuged at 16,000*g* for 15 min at 4 °C and supernatants were incubated with agarose beads coated with eIF3a antibodies at 4 °C for 3 h. Immunoprecipitants were washed at least three times with lysis buffer, followed by RNA extraction and RT–PCR.

**Puromycin labeling.** Cells at 80–90% confluence was changed with fresh medium 2 h before treated with 10 μg ml$^{-1}$ puromycin for 10 min. After washing twice with ice-cold Dulbecco's PBS, cells were lysed with SDS–PAGE sample buffer and proteins were separated on SDS–PAGE followed by immnuoblotting.

**Dual luciferase assay.** Firefly luciferase reporters were transfected into MEFs for 6 h. Transfected cells were subjected to amino acid starvation for 2 h before collection. The Luciferase Reporter Assay System (Promega) was used to measure firefly luciferase activities. Relative values of firefly luciferase activities were normalized to mRNA levels.

**Cell proliferation assays.** A total of 2,000 HEK293 T cells or MEFs per well were seeded into 96-well plates, followed by cell culture for up to 96 h. The cell viability was detected by adding 10 µl of Cell Counting Kit-8 solution (Dojindo) to each well followed by incubation at 37 °C for 1–2 h. The absorbance at the wavelength of 450 nm was detected by TECAN Spak10.

**Polysome profiling analysis.** Sucrose solutions were prepared in polysome buffer (10 mM HEPES, pH 7.4, 100 mM KCl, 5 mM $MgCl_2$ and 100 mg ml$^{-1}$ cycloheximide). A Gradient Master (BioComp Instruments) was used to prepare a 15%–45% (w/v) sucrose density gradient in a SW41 ultracentrifuge tube (Backman). Cells were lysed in polysome lysis buffer (polysome buffer and 2% Triton X-100) followed by centrifugation at 14,000 r.p.m. for 10 min at 4 °C to remove the cell debris. Five hundred milliliters of supernatant loaded onto sucrose gradients was spun for 2 h 30 min at 38,000 r.p.m. 4 °C in a SW41 rotor. Samples were fractionated at 1.5 ml min$^{-1}$ via an automated fractionation system (Isco) that continually monitors $OD_{254}$ values.

**Sucrose cushion analysis.** Cells were lysed with polysome lysis buffer. Four hundred microliters of lysates were loaded on top of 1 ml of 1 M sucrose in polysome buffer. Ribosomes were pelleted by centrifugation at 90,000 r.p.m. for 2.5 h at 4 °C using a Beckman TLA-110.6 rotor. Ribosome pellets were resolubilized for various analysis.

**eIF3-seq and Ribo-seq.** Pooled ribosome fractions were digested by *Escherichia coli* RNase I (Ambion) (100 U per 100 µl) for 1 h at 4 °C to convert polysomes into monosomes. For eIF3-seq, monosomes were immunoprecipitated with eIF3a antibody in the presence of proteinase inhibitor cocktail and 0.1 U ml$^{-1}$ SUPERase_In with agarose beads overnight. Beads were washed four times before RNA extraction. For eIF3-seq and Ribo-seq, ribosome-protected mRNA fragments were extracted using TRIzol LS reagent (Invitrogen) followed by dephosphorylation for 1 h at 37 °C in a 15 µl reaction. The products were ran on a 15% polyacrylamide TBE-urea gel (Invitrogen) and visualized using SYBR Gold (Invitrogen). Either 40–60 nucleotide (for RNA-seq) or 25–35 nucleotide (for Ribo-seq) regions were excised. RNA fragments were eluted by soaking in 400 µl of RNA elution buffer (300 mM NaOAc, pH 5.5, 1 mM EDTA, 0.1 U ml$^{-1}$ SUPERase_In) overnight. After Spin-X column (Corning) cleanup and ethanol precipitation, purified RNA fragments were resuspended in nuclease-free water. The RNA fragments were mixed with 0.15 µg linker (rApp/NNNNCTGTAGGCACCATCAAT/3ddC), heated at 70 °C for 90 s and then cooled to room temperature. Ligation was conducted at 22 °C for 3 h in a 20 µl reaction using 20 U of T4 RNA ligase 2 truncated (NEB). After heat inactivation at 80 °C for 10 min, products were resolved on a 10% polyacrylamide TBE-urea gel. Either 65–85 nucleotide (for RNA-seq) or 50–70 nucleotide (for Ribo-seq) regions were excised and RNA fragments were eluted by soaking overnight in 400 µl of RNA elution buffer. RNA fragments were precipitated by ethanol and resuspended in nuclease-free water.

For reverse transcription, the following oligos containing barcodes were used (Phos represents phosphorylation, NNN represents random sequence, SpC18 represents Hexa-ethyleneglycol spacer):

(Phos)CTANNNAGATCGGAAGAGCGTCGTGTAGGGAAAGAGTGT AGATCTCGGTGGTCGC(SpC18)CACTCA(SpC18)TTCAGACGTGTGCTCTT CCGATCTATTGATGGTGCCTACAG

(Phos)AGCNNNAGATCGGAAGAGCGTCGTGTAGGGAAAGAGTGT AGATCTCGGTGGTCGC(SpC18)CACTCA(SpC18)TTCAGACGTGTGCTCTT CCGATCTATTGATGGTGCCTACAG

(Phos)ATTNNNAGATCGGAAGAGCGTCGTGTAGGGAAAGAGTGT AGATCTCGGTGGTCGC(SpC18)CACTCA(SpC18)TTCAGACGTGTGCTCTT CCGATCTATTGATGGTGCCTACAG

(Phos)CCGNNNAGATCGGAAGAGCGTCGTGTAGGGAAAGAGTGT AGATCTCGGTGGTCGC(SpC18)CACTCA(SpC18)TTCAGACGTGTGCTCTT CCGATCTATTGATGGTGCCTACAG

The linker ligated RNA sample was mixed with 0.5 mM dNTP and 2.5 mM synthesized RT primer (and incubated at 75 °C for 5 min, followed by incubation on ice for 3 min). The reaction mixture then underwent reverse transcription with 40 U of RNaseOUT and 200 U of SuperScript III, according to the manufacturer's instructions. Reverse transcription products were separated on a 10% polyacrylamide TBE-urea gel, and a 200-nucleotide region was excised and eluted using DNA gel elution buffer (300 mM NaCl, 1 mM EDTA). cDNA was circularized in a 20 µl reaction with 100 U of CircLigase II (Epicenter) at 60 °C for 1 h, according to the manufacturer's instructions.

**Deep sequencing.** Circular DNA was amplified by PCR by using the Phusion high-fidelity (HF) enzyme (NEB) according to the manufacturer's instructions. The PCR forward primer 5′-AATGATACGGCGACCACCGAGATCTACA C-3′ and reverse primer 5′-CAAGCAGAAGACGGCATACGAGATG TGACTGGAGTTCAGACGTGTGCTCTTCCG-3′ were used to create DNA suitable for sequencing. PCR was carried out with an initial 30 s denaturation at 98 °C, followed by 12 cycles of 10 s at 98 °C, 20 s at 65 °C and 20 s at 72 °C. PCR products were resolved on a nondenaturing 8% polyacrylamide TBE gel. Expected DNA at 180 bp was excised and precipitated. After quantification using the Agilent BioAnalyzer DNA 1000 assay, equal amounts of samples (5 pM) were pooled into one sequencing lane followed by sequencing by using sequencing primer 5′-CGACAGGTTCAGAGTTCTACAGTCCGACGATC-3′ (Illumina HiSeq).

**Sequencing reads alignment.** The 3′ adapter CTGTAGGCACCATCAAT and low-quality bases were trimmed by Cutadapt. The trimmed reads with a length <15 nucleotides were excluded. The remaining reads were mapped to the mouse transcriptome (ENSEMBL database, GRCm38) using Bowtie with parameters: -a--best -m1--strata. For each gene, the mRNA with longest CDS was selected for analysis. In the case of equal CDS lengths, the longest transcript was chosen. For read alignment, a maximum of two mismatches were permitted. To avoid ambiguous, the reads that were mapped to multiple positions were excluded.

**Aggregation plot around translation start and stop codon.** First, ribosome P-site was defined as the position +12, +13 and +14 from the 5′-end of the reads (the first position of the reads is recorded as 0). Then, for each mRNA, footprint reads in CDS were counted, the mRNAs with total reads in CDS < 16 or the empty codons (no observed reads) >90% were excluded. A count per million value at each codon in CDS or triplet in UTRs was calculated by dividing the count at the codon/triplet by the count of total aligned reads. Count per million values with the same distance from the start or stop codon was averaged over the whole transcriptome.

**Footprint reads in different mRNA regions.** We divided mRNA into different segments: 5′-UTR, start codon proximal (from start codon to downstream 500 nucleotides), CDS and 3′-UTR. We counted footprint reads located to different mRNA segments respectively. A start codon density was calculated by dividing the count in the start codon proximal region by the read count in remaining CDS. mRNAs with CDS < 700 nucleotides or total read count in CDS < 16 were excluded. To estimate the reinitiation density from 3′-UTR, the ratio of 3′-UTR over CDS was calculated, and the ratio of 5′-UTR over CDS was used as a background control.

**Estimation of ribosome density on mRNAs.** For each mRNAs, a calculated reads per kilobase of transcript, per million mapped reads (RPKM) value was used to measure the relative ribosome density on individual mRNAs. mRNAs with RPKM value <1 were excluded.

**GO analyses.** mRNAs enriched with eIF3-associated 80S ribosomes (that is fold change of RPKM value from eIF3-seq over RPKM value from Ribo-seq is >2) were used for GO analysis. The whole mouse transcriptome was used as a background. GO analyses were performed by DAVID GO.

**Statistical analysis.** Results are expressed as mean ± s.d. Comparisons between groups were made by two-way ANOVA and unpaired two-tailed Student's *t*-test.

**Reporting Summary.** Further information on research design is available in the Nature Research Reporting Summary linked to this article.

## Data availability

All sequencing data have been deposited in the Gene Expression Omnibus under accession number GSE181040. Source data are provided with this paper.

## Code availability

All the codes used in this study can be found in https://github.com/QianLab-Cornell/Count_Ribo_Reads.git

## References

40. Sanjana, N. E., Shalem, O. & Zhang, F. Improved vectors and genome-wide libraries for CRISPR screening. *Nat. Methods* **11**, 783–784 (2014).
41. Shalem, O. et al. Genome-scale CRISPR–Cas9 knockout screening in human cells. *Science* **343**, 84–87 (2014).

## Acknowledgements

We thank N. E. Zachara for providing inducible MEF *Ogt* KO cell lines and R. C. Wek for ATF4 uORF mutants. We also thank Qian lab members for helpful discussions. We are grateful to Cornell University Life Sciences Core Laboratory Center for sequencing support. We thank the Proteomic and MS Facility of Cornell University for help with the mass spectrometry. This work was supported by US National Institutes of Health (R01GM1222814 and DP1GM142101) and HHMI Faculty Scholar (55108556) to S.-B.Q.

## Author contributions

S.-B.Q. conceived the project and designed the experiments. X.E.S. designed and performed the majority of experiments. Y.M. conducted the majority of sequencing data analysis. L.J. assisted HiBiT reporter assay and Ribo-seq experiments. All authors discussed the results and edited the manuscript.

## Competing interests

The authors declare no competing interests.

## Additional information

**Extended data** is available for this paper at https://doi.org/10.1038/s41589-021-00913-4.

**Supplementary information** The online version contains supplementary material available at https://doi.org/10.1038/s41589-021-00913-4.

**Correspondence and requests for materials** should be addressed to Shu-Bing Qian.

**Peer review information** *Nature Chemical Biology* thanks Wen Yi and other, anonymous, reviewer(s) for their contribution to the peer review of this work.

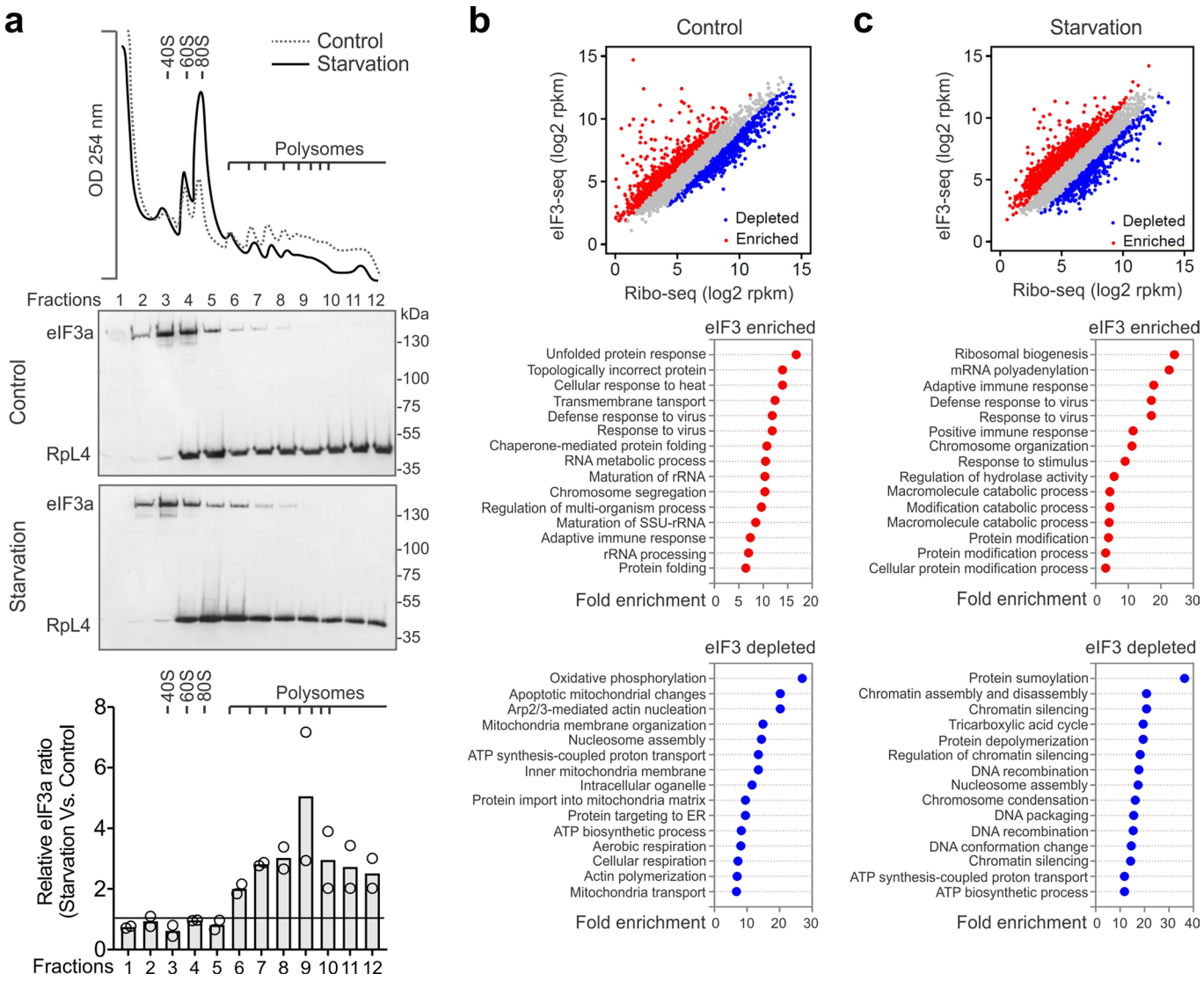


**Extended Data Fig. 1 | Characterization of eIF3-80S association in response to amino acid starvation. a**. MEFs with or without amino acid starvation for 2 hr were subjected polysome profiling using sucrose gradient. Ribosome fractions were collected for immunoblotted using antibodies indicated. The bottom panel shows the eIF3a levels relative to the RpL4. Error bars, mean ± s.e.m.; t-test, two-tailed; n = 2 independent experiments. **b**. The top panel shows a scatter plot of read density on individual transcripts between 80 S (Ribo-seq, x-axis) and eIF3-80S (eIF3-seq, y-axis) footprints from MEF cells. The bottom panel shows the GO analysis of eIF3-enriched (red) or eIF3-depleted (blue) transcripts. **c**. The top panel shows a scatter plot of read density on individual transcripts between 80 S (Ribo-seq, x-axis) and eIF3-80S (eIF3-seq, y-axis) footprints from MEF cells subjected to amino acid starvation for 2 hr. The bottom panel shows the GO analysis of eIF3-enriched (red) or eIF3-depleted (blue) transcripts.

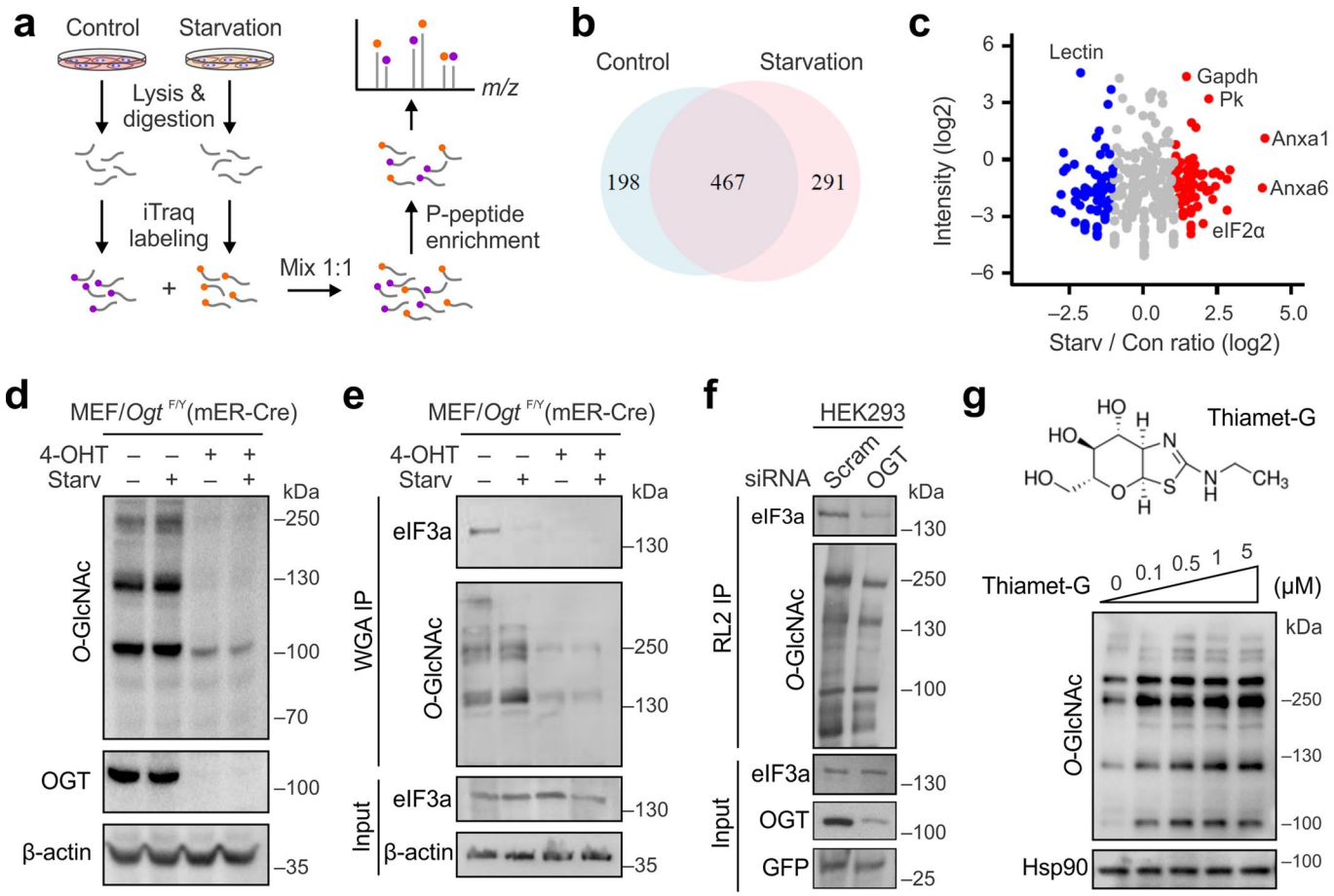


**Extended Data Fig. 2 | Amino acid starvation induces de-O-GlcNAcylation of eIF3a. a**. Schematic of quantitative mass spectrometry using iTRAQ to compare phosphoproteomics. **b**. A venn diagram shows the number of proteins identified in control (198), 2 hr amino acid starvation (291), or both (467) from the phosphoproteomics data in (A). **c**. A scatter plot shows the differential phosphoproteins in MEF cells with and without amino acid starvation. Phosphoproteins with >2 fold increase or decrease are colored in red and blue, respectively. **d**. MEF/Ogt F/Y(mER-Cre) cells were pre-treated with (+) or without (–) 0.5 μM 4-OHT for 24 hr followed by normal media for another 24 hr. Cells were then subjected to amino acid starvation for 2 hr prior to immunoblotting. Representative results of 3 independent experiments were shown. **e**. MEF cells as in (D) were subjected to immunoprecipitation using WGA antibody followed by immunoblotting. Representative results of 3 independent experiments were shown. **f**. HEK293 cells were transfected with scramble or siRNA targeting OGT for 24 hr followed by RL2 (O-GlcNAc) immunoprecipitation and immunoblotting. Representative results of 3 independent experiments were shown. **g**. MEF cells were treated with increasing doses of Thiamet-G for 16 hr followed by immunoblotting. Representative results of 3 independent experiments were shown.

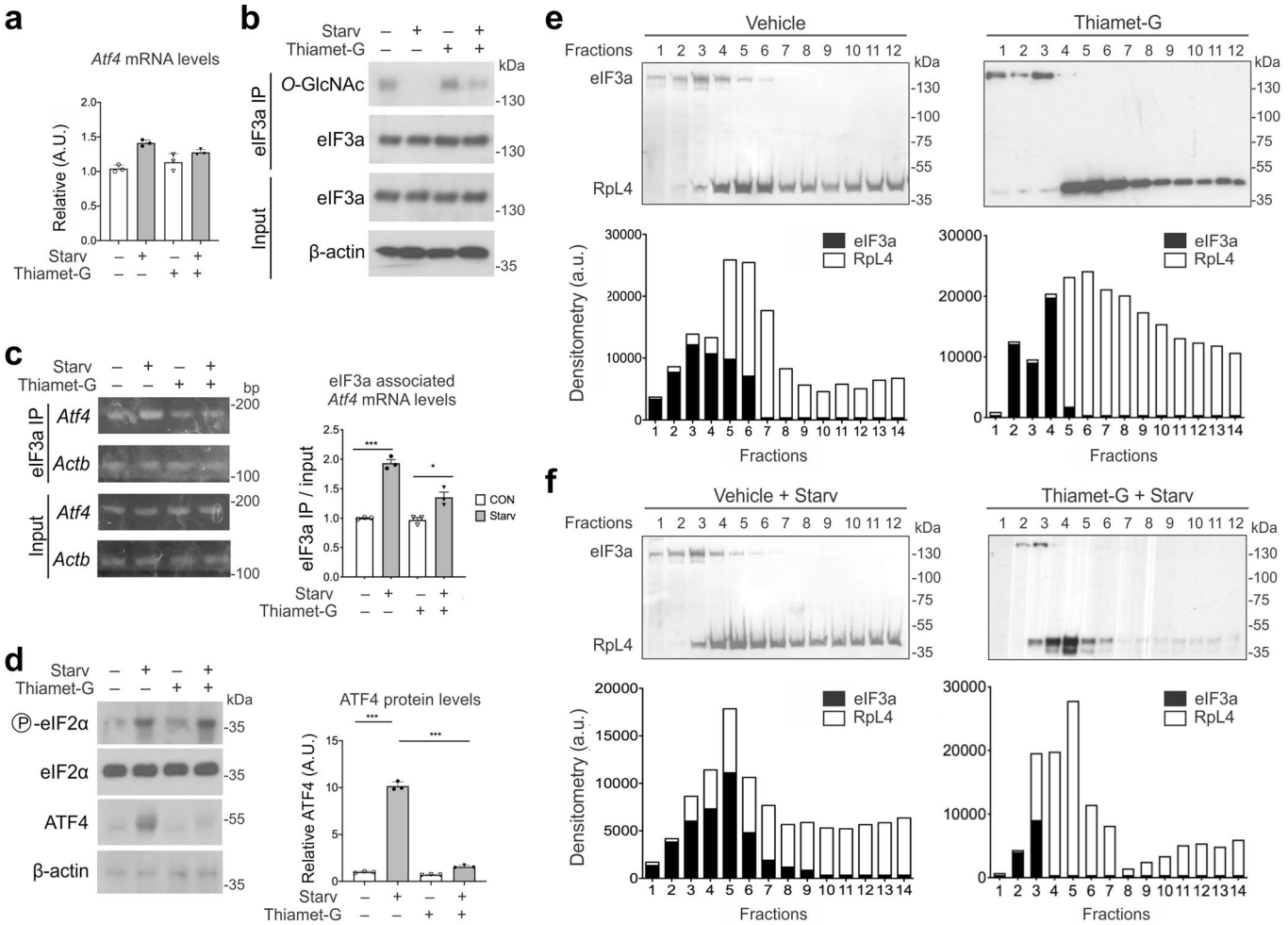


**Extended Data Fig. 3 | Characterization of eIF3-80S association in the presence of Thiamet-G. a**. MEF cells were treated with Thiamet-G for 16 hr with or without amino acid starvation for 2 hr followed by RNA extraction and RT-qPCR. Relative Atf4 mRNA levels are normalized to the Actb mRNA level. Error bars, mean ± s.d.; n = 3 independent experiments. **b**. MEF cells were treated with 0.4 μM Thiamet-G for 1 hr followed by amino acid starvation for 2 hr. Whole-cell lysates were immunoprecipitated using the eIF3a antibody followed by immunoblotting using indicated antibodies. Representative results of 3 independent experiments were shown. **c**. Same as (b), total RNAs and eIF3-associated RNAs were extracted followed by RT-PCR measuring Actb and Aft4 mRNA levels. Relative Atf4/Actb ratios were normalized to the corresponding input. Error bars, mean ± s.d.; *p = 0.019; ***p = 0.00078; two-way ANOVA; n = 3 independent experiments. **d**. MEF cells as in (b) were subjected to immunoblotting using antibodies indicated. The right panel shows the relative ATF4 protein levels normalized to α-tubulin. Error bars, mean ± s.d.; ***p = 0.00014; two-way ANOVA; n = 3 independent experiments. **e**. MEF cells were treated with Thiamet-G for 16 hr were subjected to polysome profiling using sucrose gradient. Ribosome fractions were collected for immunoblotted using antibodies indicated. The bottom panel shows the densitometry of eIF3a and RpL4 protein levels. Representative results of 3 independent experiments were shown. **f**. MEF cells as (e) were subjected to amino acid starvation for 2 h followed by polysome profiling using sucrose gradient. Ribosome fractions were collected for immunoblotted using antibodies indicated. The bottom panel shows the densitometry of eIF3a and RpL4 protein levels. Representative results of 3 independent experiments were shown.

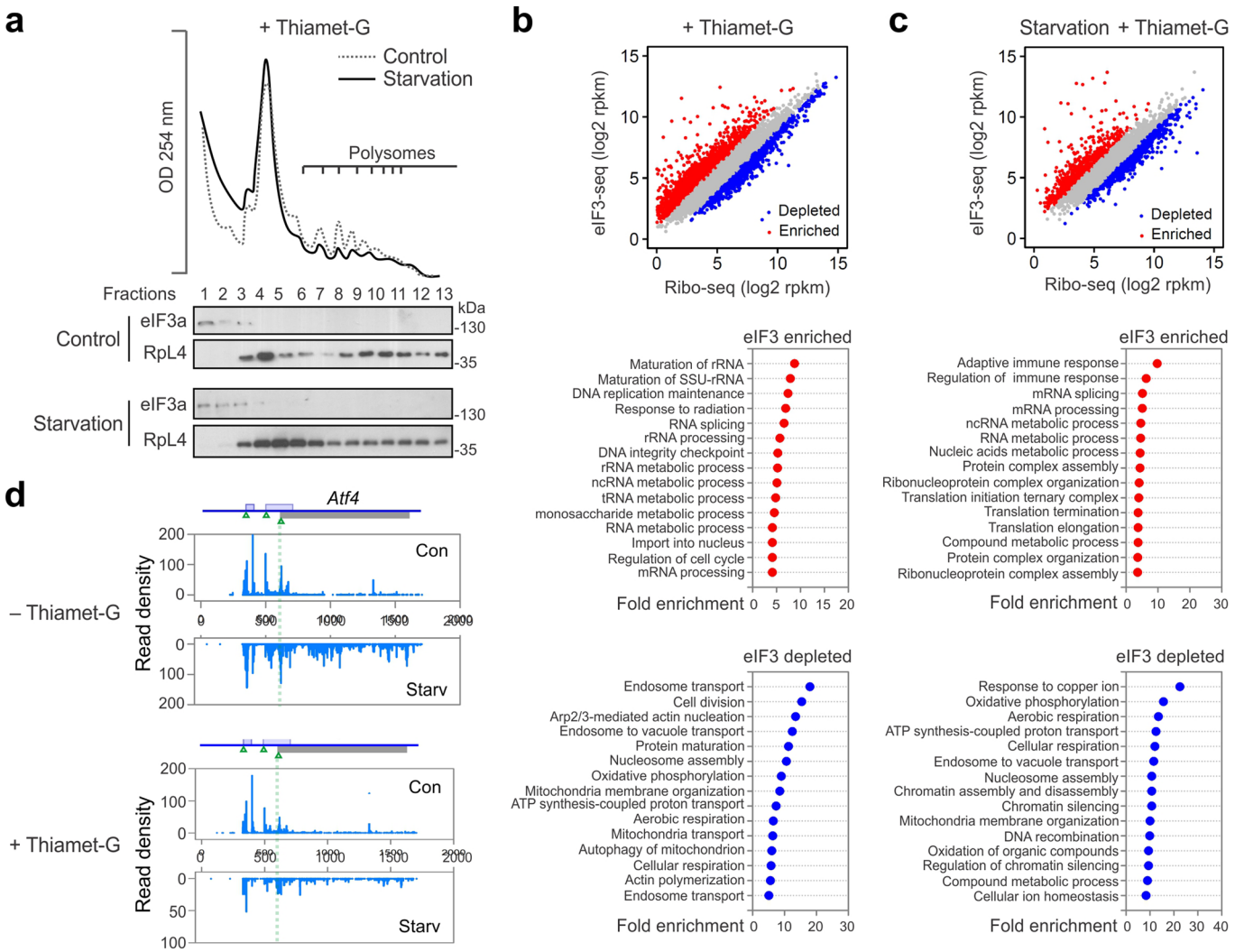


**Extended Data Fig. 4 | Further characterization of eIF3-80S association in the presence of Thiamet-G. a**. MEF cells were treated with Thiamet-G for 16 hr followed by amino acid starvation for 2 hr. Polysome profiling was conducted using sucrose gradient. Ribosome fractions were collected for immunoblotted using antibodies indicated. Representative results of 3 independent experiments were shown. **b**. The top panel shows a scatter plot of read density on individual transcripts between 80 S (Ribo-seq, x-axis) and eIF3-80S (eIF3-seq, y-axis) footprints from MEF cells treated with Thiamet-G. The bottom panel shows the GO analysis of eIF3-enriched (red) or eIF3-depleted (blue) transcripts. **c**. The top panel shows a scatter plot of read density on individual transcripts between 80 S (Ribo-seq, x-axis) and eIF3-80S (eIF3-seq, y-axis) footprints from MEF cells treated with Thiamet-G and 2 hr amino acid starvation. The bottom panel shows the GO analysis of eIF3-enriched (red) or eIF3-depleted (blue) transcripts. **d**. The distribution of 80 S footprints in the Atf4 transcript from MEF cells with or without Thiamet-G treatment, before and after amino acid starvation.

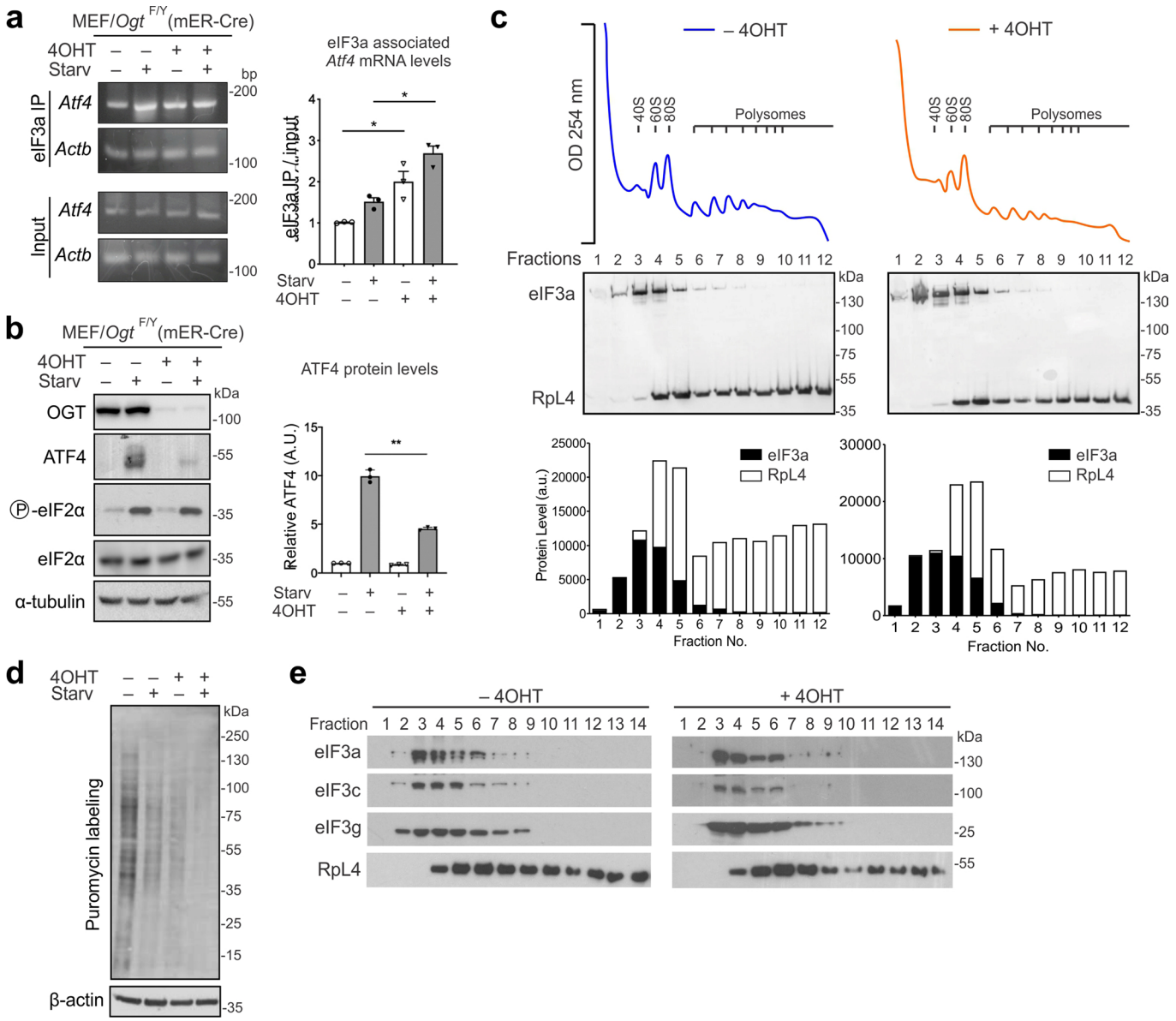


**Extended Data Fig. 5 | Deficient O-GlcNAcylation attenuates global protein synthesis. a**. MEF/Ogt F/Y(mER-Cre) cells were pre-treated with (+) or without (–) 0.5 μM 4-OHT for 24 hr followed by normal media for another 24 hr. Cells were then subjected to amino acid starvation for 2 hr followed by immunoprecipitation using the eIF3a antibody. Total RNAs and eIF3-associated RNAs were extracted followed by RT-PCR measuring Actb and Aft4 mRNA levels. Relative Atf4/Actb ratios were normalized to the corresponding input. Error bars, mean ± s.e.m.; *P = 0.0036; two-way ANOVA; n = 3 independent experiments. **b**. MEF cells as in (a) were subjected to immunoblotting using antibodies indicated. The right panel shows the relative ATF4 protein levels normalized to α-tubulin. Error bars, mean ± s.e.m.; *P = 0.015, **P = 0.0067; two-way ANOVA; n = 3 independent experiments. **c**. MEF cells as in (a) were subjected to polysome profiling using sucrose gradient. Ribosome fractions were collected for immunoblotted using antibodies indicated. The bottom panel shows the eIF3a levels relative to the RpL4. Error bars, mean ± s.e.m.; t-test, two-tailed; n = 2 independent experiments. The bottom panel shows the densitometry of eIF3a and RpL4 protein levels. **d**. MEF cells as in (a) were incubated with 200 ng/μl of puromycin for 15 min. Whole cell lysates were used for immunoblotting. Representative results of 3 independent experiments were shown. **e**. MEF cells as in (a) were subjected to polysome profiling using sucrose gradient. Ribosome fractions were collected for immunoblotted using antibodies indicated. Representative results of 3 independent experiments were shown.

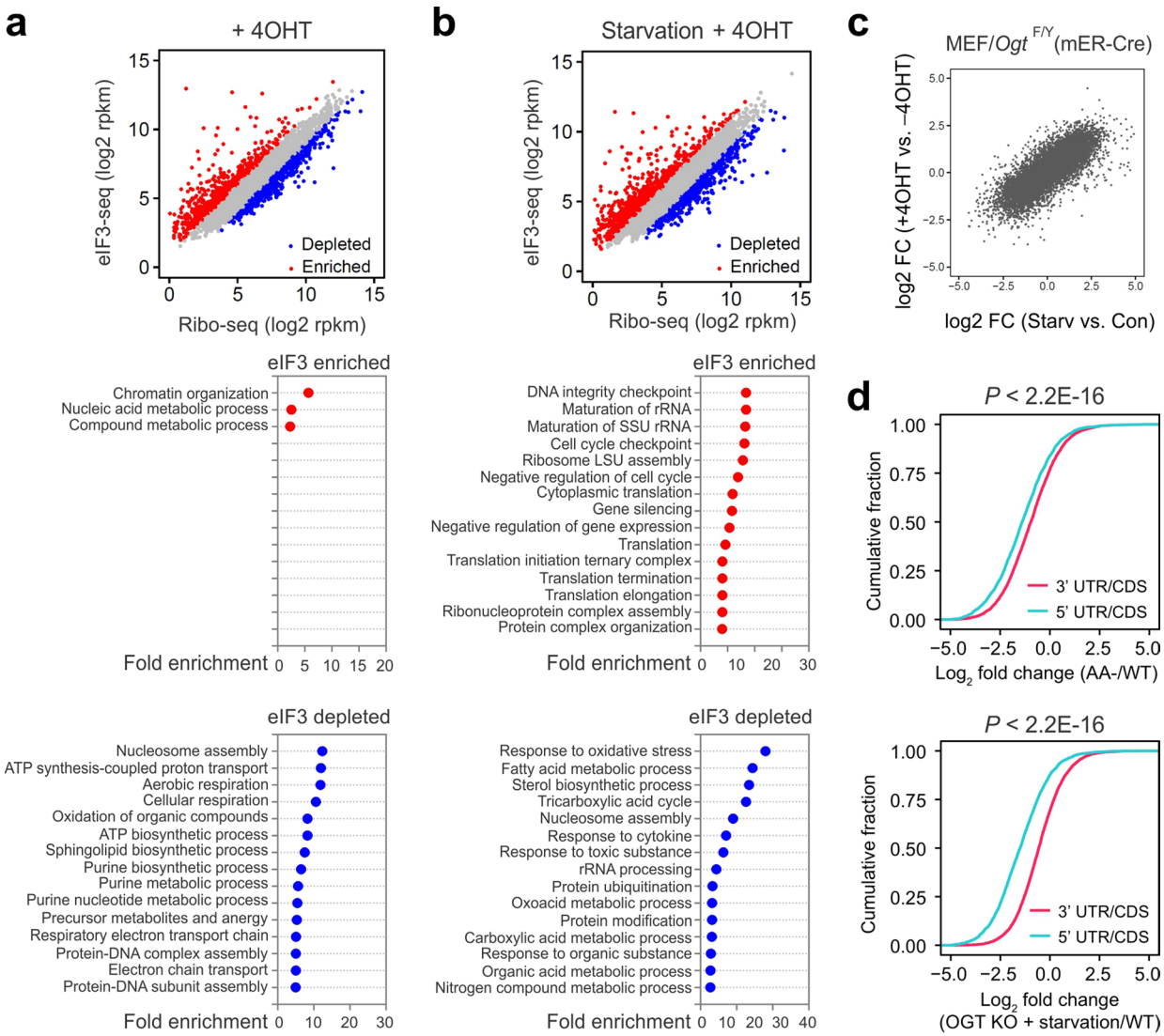


**Extended Data Fig. 6 | Deficient O-GlcNAcylation of eIF3a promotes eIF3-80S association. a**. The top panel shows a scatter plot of read density on individual transcripts between 80 S (Ribo-seq, x-axis) and eIF3-80S (eIF3-seq, y-axis) footprints from MEF cells with 4-OHT treatment. The bottom panel shows the GO analysis of eIF3-enriched (red) or eIF3-depleted (blue) transcripts. **b**. The top panel shows a scatter plot of read density on individual transcripts between 80 S (Ribo-seq, x-axis) and eIF3-80S (eIF3-seq, y-axis) footprints from MEF cells with 4-OHT treatment and 2 hr amino acid starvation. The bottom panel shows the GO analysis of eIF3-enriched (red) or eIF3-depleted (blue) transcripts. **c**. A Scatter plot shows the correlation of fold changes (log2) of CDS ribosome density in MEF/Ogt F/Y(mER-Cre) cells between Ogt knockout and amino acid starvation. **d**. Cumulative distribution of fold changes of read density in 5'UTR (blue) and 3'UTR (red) relative to the CDS in MEF cells with OGT knockout (top panel) or together with amino acid starvation (bottom panel). P values are based on Wilcoxon signed-rank test.

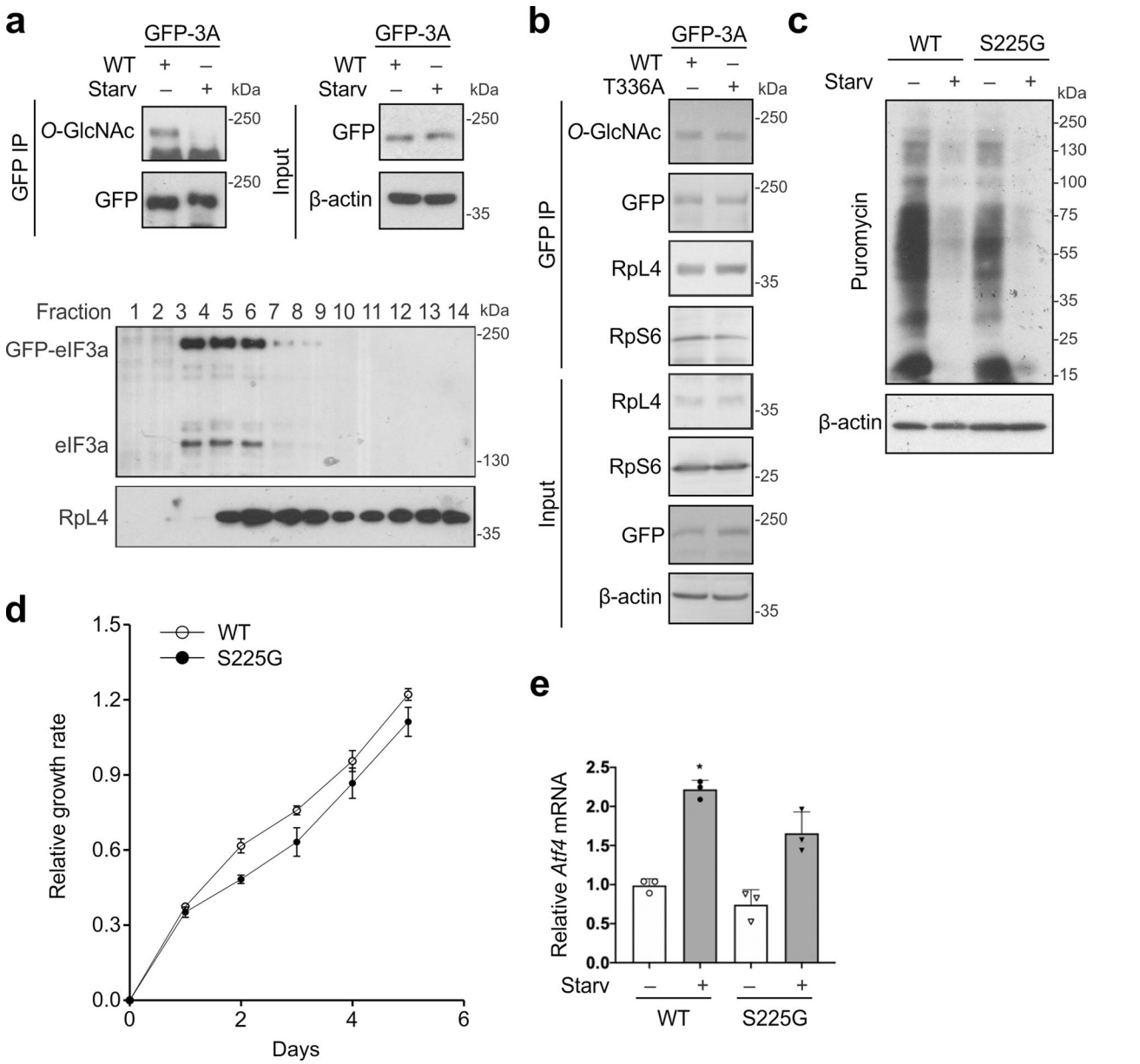


**Extended Data Fig. 7 | Characterization of eIF3a mutants with deficient O-GlcNAcylation. a**. HEK 293 cells were transfected with plasmids expressing EGFP-eIF3a for 24 hr. Cells lysates were immunoprecipitated using an anti-GFP antibody followed by immunoblotting. Bottom panel, HEK cells transfected with GFP-eIF3a were subjected to a 15%-45% sucrose gradient, followed by western blotting using indicated antibodies. Representative results of 3 independent experiments were shown. **b**. HEK 293 cells were transfected with plasmids expressing wild type eIF3a (WT) or T336A mutant fused to EGFP for 24 hr. Cells lysates were immunoprecipitated using an anti-GFP antibody followed by immunoblotting. Representative results of 3 independent experiments were shown. **c**. HEK 293 cells bearing eIF3a wildtype (WT) and S225G mutation were incubated with 200 ng/μl of puromycin for 15 min. Whole cell lysates were used for immunoblotting. **d**. Growth rates of HEK 293 cells bearing eIF3a wildtype (WT) and S225G mutation were measured using CCK-8 assay. Error bars, mean ± s.d.; t-test, two-tailed; n = 3 biological replicates. **e**. HEK293 cells as in (C) were subjected to amino acid starvation for 2 hr followed by total RNA extraction and RT-qPCR. Relative Atf4 mRNA levels are normalized to the Actb mRNA level. Error bars, mean ± s.d.; n = 3 independent experiments.

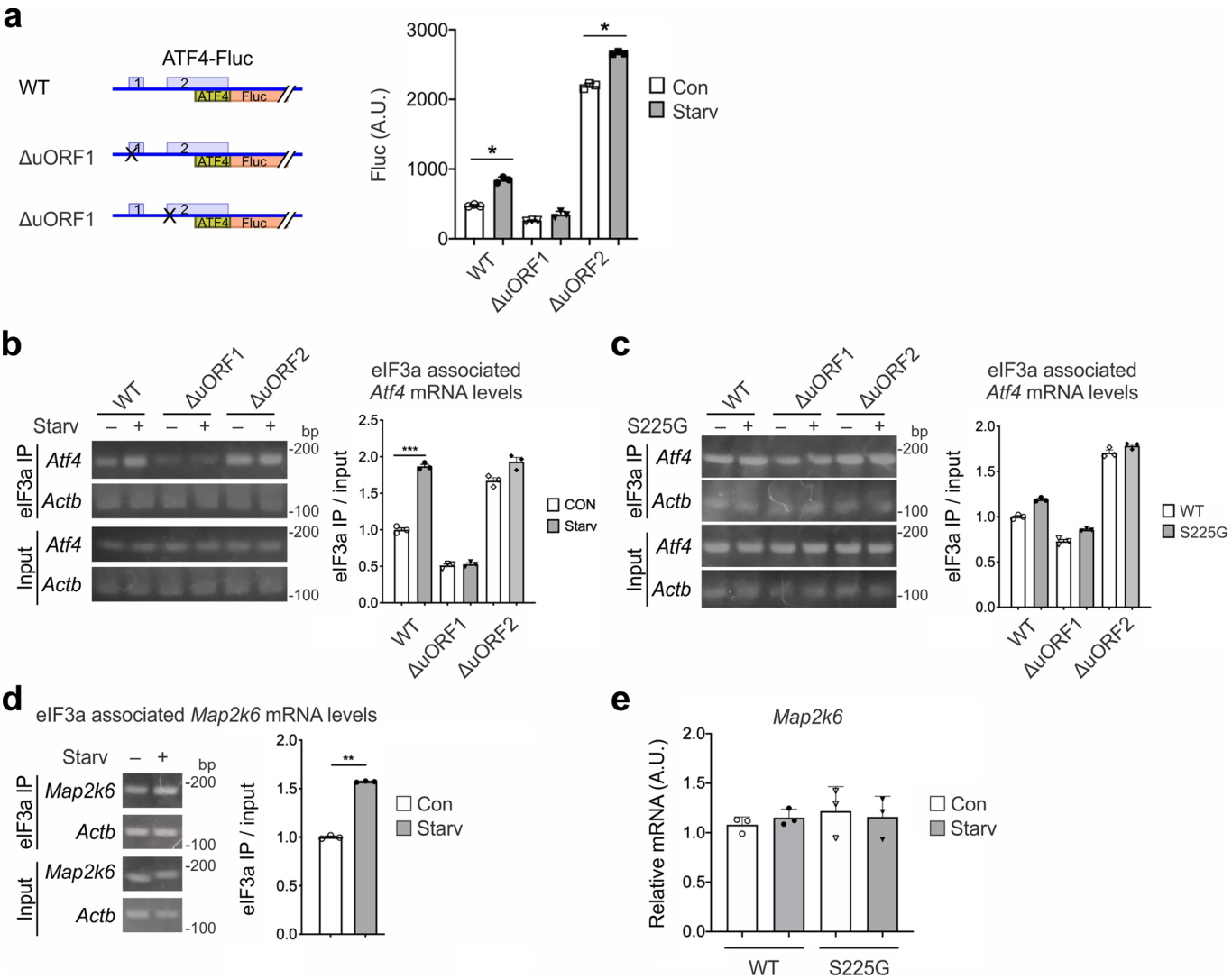


**Extended Data Fig. 8 | Deficient O-GlcNAcylation of eIF3a affects general translation reinitiation. a**. The left panel shows the schematic of ATF4-Fluc reporters with uORF deletion. The right panel shows the Fluc activities in transfected MEF cells with and without amino acid starvation. Error bars, mean ± s.d.; *p = 0.037; two-way ANOVA; n = 3 independent experiments. **b**. MEF cells transfected with ATF4-Fluc reporter mutants were subjected to amino acid starvation for 2 hr. Whole cell lysates were immunoprecipitated using the eIF3a antibody. Total RNAs and eIF3-associated RNAs were extracted followed by RT-PCR measuring Actb and Aft4 mRNA levels. Relative Atf4/Actb ratios were normalized to the corresponding input. Error bars, mean ± s.d.; ***p = 0.00035; two-way ANOVA; n = 3 independent experiments. **c**. HEK293 cells bearing S225G mutation of eIF3a were transfected with ATF4-Fluc reporter mutants followed by amino acid starvation for 2 hr. Whole cell lysates were immunoprecipitated using the eIF3a antibody. Total RNAs and eIF3-associated RNAs were extracted followed by RT-PCR measuring Actb and Aft4 mRNA levels. Relative Atf4/Actb ratios were normalized to the corresponding input. Error bars, mean ± s.d.; n = 3 independent experiments. **d**. EK293 cells with (+) or without (–) amino acid starvation for 2 hr were subjected to immuno-precipitation using eIF3a antibody. Total RNAs and eIF3-associated RNAs were extracted followed by RT-PCR measuring Actb and Map2k6 mRNA levels. Relative Map2k6/Actb ratios were normalized to the corresponding input. Error bars, mean ± s.d.; *p = 0.018; two-way ANOVA; n = 3 independent experiments. **e**. Steady-state mRNA levels of Map2k6 in HEK293 cells as in (d) were normalized with Actb, Error bars, mean ± s.d.; n = 3 independent experiments.

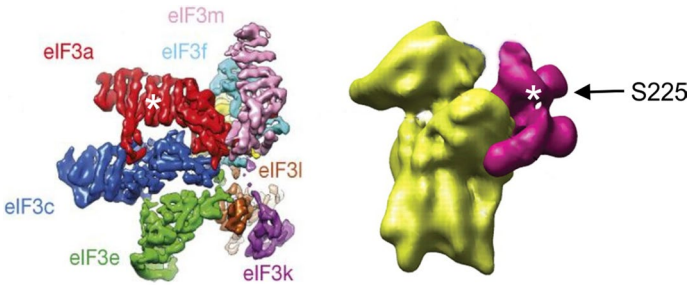


**Extended Data Fig. 9 | A model summarizing eIF3-80S complex association orchestrated by dynamic O-GlcNAcylation of eIF3a.** Schematic Cryo-EM structure of mammalian eIF3 (Adopted from des Georges et al. 2015). eIF3a is shown in red and the putative O-GlcNAc modification site shown as the white star.

nature research

Corresponding author(s): Shu-Bing Qian

Last updated by author(s): Sep 17, 2021

# Reporting Summary

Nature Research wishes to improve the reproducibility of the work that we publish. This form provides structure for consistency and transparency in reporting. For further information on Nature Research policies, see our Editorial Policies and the Editorial Policy Checklist.

## Statistics

For all statistical analyses, confirm that the following items are present in the figure legend, table legend, main text, or Methods section.

| n/a | Confirmed | |
|---|---|---|
| ☐ | ☒ | The exact sample size (*n*) for each experimental group/condition, given as a discrete number and unit of measurement |
| ☐ | ☒ | A statement on whether measurements were taken from distinct samples or whether the same sample was measured repeatedly |
| ☐ | ☒ | The statistical test(s) used AND whether they are one- or two-sided<br>*Only common tests should be described solely by name; describe more complex techniques in the Methods section.* |
| ☒ | ☐ | A description of all covariates tested |
| ☒ | ☐ | A description of any assumptions or corrections, such as tests of normality and adjustment for multiple comparisons |
| ☐ | ☒ | A full description of the statistical parameters including central tendency (e.g. means) or other basic estimates (e.g. regression coefficient) AND variation (e.g. standard deviation) or associated estimates of uncertainty (e.g. confidence intervals) |
| ☐ | ☒ | For null hypothesis testing, the test statistic (e.g. *F*, *t*, *r*) with confidence intervals, effect sizes, degrees of freedom and *P* value noted<br>*Give P values as exact values whenever suitable.* |
| ☒ | ☐ | For Bayesian analysis, information on the choice of priors and Markov chain Monte Carlo settings |
| ☒ | ☐ | For hierarchical and complex designs, identification of the appropriate level for tests and full reporting of outcomes |
| ☒ | ☐ | Estimates of effect sizes (e.g. Cohen's *d*, Pearson's *r*), indicating how they were calculated |

*Our web collection on statistics for biologists contains articles on many of the points above.*

## Software and code

Policy information about availability of computer code

| | |
|---|---|
| Data collection | NA |
| Data analysis | Cutadapt v1.18 was used to filter low quality reads. Bowtie v1.1.2 and STAR v2.7.0 were used to align reads to the human and mouse transcriptome. R v3.5.1 was used to perform all statistical analysis. ggplot2 for R was used to make all statistical figures. The custom Perl scripts were used to analyze all sequencing data, which are available on request to the corresponding authors. |

For manuscripts utilizing custom algorithms or software that are central to the research but not yet described in published literature, software must be made available to editors and reviewers. We strongly encourage code deposition in a community repository (e.g. GitHub). See the Nature Research guidelines for submitting code & software for further information.

## Data

Policy information about availability of data

All manuscripts must include a data availability statement. This statement should provide the following information, where applicable:

- Accession codes, unique identifiers, or web links for publicly available datasets
- A list of figures that have associated raw data
- A description of any restrictions on data availability

All new sequencing data that support the findings of this study have been deposited in the National Center for Biotechnology Information Gene Expression Omnibus (GEO) and are accessible through the GEO Series accession number GSE181040. All other relevant data are available from the corresponding author on request.

# Field-specific reporting

Please select the one below that is the best fit for your research. If you are not sure, read the appropriate sections before making your selection.

☒ Life sciences ☐ Behavioural & social sciences ☐ Ecological, evolutionary & environmental sciences

For a reference copy of the document with all sections, see nature.com/documents/nr-reporting-summary-flat.pdf

# Life sciences study design

All studies must disclose on these points even when the disclosure is negative.

| | |
|---|---|
| Sample size | No sample size was per-determined. Three or more independent results were used to perform statistical analysis. Two or more biological replicates for sequencing Ribo-seq were performed. All sample sizes and the number of replicates were stated in figure legends. |
| Data exclusions | No data exclusion |
| Replication | Experiments in this study were reproduced at least three times. Replication were described in figure legends. |
| Randomization | All experiments were performed on cell lines, and no animal studies were performed. Cells from each cell line have the same genetic background and phenotype, hence no randomization was used. |
| Blinding | Investigators were blinded to group allocation during data collection and analysis. |

# Reporting for specific materials, systems and methods

We require information from authors about some types of materials, experimental systems and methods used in many studies. Here, indicate whether each material, system or method listed is relevant to your study. If you are not sure if a list item applies to your research, read the appropriate section before selecting a response.

## Materials & experimental systems

| n/a | Involved in the study |
|---|---|
| ☐ | ☒ Antibodies |
| ☐ | ☒ Eukaryotic cell lines |
| ☒ | ☐ Palaeontology and archaeology |
| ☒ | ☐ Animals and other organisms |
| ☒ | ☐ Human research participants |
| ☒ | ☐ Clinical data |
| ☒ | ☐ Dual use research of concern |

## Methods

| n/a | Involved in the study |
|---|---|
| ☒ | ☐ ChIP-seq |
| ☒ | ☐ Flow cytometry |
| ☒ | ☐ MRI-based neuroimaging |

# Antibodies

| | |
|---|---|
| Antibodies used | Anti-rabbit IgG eIF3A (3411), anti-rabbit IgG RPS6 (2217), anti-rabbit IgG p-eIF2α Ser51 (3398), anti-rabbit IgG eIF2α (9722), anti-rabbit IgG MMK6/MAP2K6 (9264), anti-rabbit IgG eIF3C (2068), and anti-rabbit IgG ATF4 (11815) were purchased from Cell Signaling. Anti-mouse IgG O-GlcNAc (RL2, MA1-072) was purchased from Fisher Scientific; anti-mouse IgG Puromycin (PMY-2A4) was purchased from Developmental Studies Hybridoma Bank; anti-mouse IgG β-actin (F1804) from Sigma; anti-rabbit IgG OGT (11576-2-AP), anti-rabbit IgG eIF3g (11165-1-AP) and anti-rabbit IgG RPL4 (11302-1-AP) from Proteintech; anti-rabbit IgG GFP (NB600-308) from Novus |
| Validation | All antibodies used were verified by the manufacture and were independently tested/verified by the authors as follows:<br>Cell signaling:<br>Anti-rabbit IgG eIF3A (3411): Company website application listed: WB, IP, IF, IHC in H M R Mk; Application tested in the manuscript: WB (1:1000), IP (1:50) in human and mouse<br>Anti-rabbit IgG RPS6 (2217): Company website application listed: WB, IHC, IF in H M R Mk; Application tested in the manuscript:WB (1:1000) in human and mouse<br>Anti-rabbit IgG p-eIF2α Ser51 (3398): Company website application listed:WB, IP, IHC in H M R Mk Dm; Application tested in the manuscript:WB (1:1000) in human and mouse<br>Anti-rabbit IgG eIF2α (9722): Company website application listed:WB in H M R Mk; Application tested in the manuscript:WB (1:1000) in human and mouse<br>Anti-rabbit IgG MMK6/MAP2K6 (9264): Company website application listed:WB, IP in H M R; Application tested in the manuscript:WB (1:1000) in human and mouse<br>Anti-rabbit IgG eIF3C (2068): Company website application listed:WB in H M Mk; Application tested in the manuscript:WB (1:1000) in human and mouse<br>Anti-rabbit IgG ATF4 (11815): Company website application listed:WB, IP, IHC, IF in H M R; Application tested in the manuscript:WB |

(1:1000) in human and mouse

Fisher Scientific:

Anti-mouse IgG O-GlcNAc (RL2, MA1-072): Company website application listed: WB, IHC, CHIP, IF in amphibian, Bovine, Chemical, Fish, Fruit fly, Hamster, Human, Invertibrate, Mouse, Non-human primate, Rat; Application tested in the manuscript: WB (1:1000), IP (1:40) in human and mouse

Developmental Studies Hybridoma Bank: Company website application listed: Application tested in the manuscript:

Anti-mouse IgG Puromycin (PMY-2A4): Company website application listed: WB, IP, ELISA, FASC in all; Application tested in the manuscript: WB (1:100) in human and mouse

Sigma:

anti-mouse IgG β-actin (F1804): Company website application listed: IF, ELISA, WB. Application tested in the manuscript: WB (1:5000) in human and mouse

Proteintech:

Anti-rabbit IgG OGT (11576-2-AP): Company website application listed: WB, IP, IHC, IF, ELISA in Human, Mouse, Rat; Application tested in the manuscript: WB (1:1000) in human and mouse

Anti-rabbit IgG eIF3g (11165-1-AP): Company website application listed: WB, IHC, IF in Human, Mouse; Application tested in the manuscript: WB (1:1000) in human and mouse

Anti-rabbit IgG RPL4 (11302-1-AP): Company website application listed: WB, IP, IHC, IF, FC, ELISA in Human, Mouse, Rat, Monkey; Application tested in the manuscript: WB (1:2000) in human and mouse

Novus:

Anti-rabbit IgG GFP (NB600-308): Company website application listed: ELISA, IHC-Fr, ICC, IHC-P, IP, WB, IHC, Electron Microscopy in species independent; Application tested in the manuscript: WB (1:2000) in transfected human and mouse

Key:

WB-Western Blot IP-Immunoprecipitation IHC-Immunohistochemistry ChIP-Chromatin Immunoprecipitation IF-Immunofluorescence F-Flow Cytometry E-P-ELISA-Peptide

H-Human M-Mouse R-Rat Hm-Hamster Mk-Monkey Vir-Virus Mi-Mink C-Chicken Dm-D. melanogaster X-Xenopus Z-Zebrafish B-Bovine Dg-Dog Pg-Pig Sc-S. cerevisiae Ce-C. elegans Hr-Horse All-All Species Expected

## Eukaryotic cell lines

Policy information about cell lines

| | |
|---|---|
| Cell line source(s) | OgtF/Y(mER-Cre) MEFs were kindly provided by Natasha E. Zachara (The Johns Hopkins University School of Medicine); HEK 293 cells were purchased from ATCC; HeLa cells were purchased from ATCC. |
| Authentication | Cells were not authenticated recently but OgtF/Y(mER-Cre) MEFs were indirectly authenticated via deep sequencing. |
| Mycoplasma contamination | Cell lines were not tested for mycoplasma contamination recently. |
| Commonly misidentified lines (See ICLAC register) | No commonly misidentified cell lines were used in this study |